

# Effect of $\beta$ -Ketoiminato Ancillary Ligand Modification on Emissive Properties of New Iridium Complexes

Ewelina Witkowska,<sup>†</sup> Bartosz Orwat,<sup>‡,§</sup> Myong Joon Oh,<sup>‡,§</sup> Gabriela Wiosna-Salyga,<sup>\*,†</sup> Ireneusz Glowacki,<sup>†</sup> Ireneusz Kownacki,<sup>\*,‡,§</sup> Kamila Jankowska,<sup>‡,§</sup> Maciej Kubicki,<sup>‡,§</sup> Blazej Gierczyk,<sup>‡</sup> Michal Dutkiewicz,<sup>§,||</sup> Izabela Grzelak,<sup>‡</sup> Marcin Hoffmann,<sup>‡</sup> Julita Nawrocik,<sup>‡,§</sup> Grzegorz Krajewski,<sup>‡,§</sup> Jacek Ulanski,<sup>†</sup> Przemyslaw Ledwon,<sup>⊥</sup> and Mieczyslaw Lapkowski<sup>⊥,#</sup>

<sup>†</sup>Department of Molecular Physics, Lodz University of Technology, Zeromskiego 116, 90-924 Lodz, Poland

<sup>‡</sup>Faculty of Chemistry, Adam Mickiewicz University in Poznan, St. Uniwersytetu Poznanskiego 8, 61-614 Poznan, Poland

<sup>§</sup>Center for Advanced Technology, Adam Mickiewicz University in Poznan, St. Uniwersytetu Poznanskiego 10, 61-614 Poznan, Poland

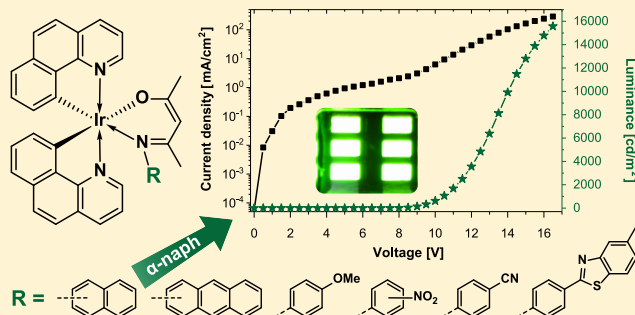
<sup>||</sup>Poznan Science and Technology Park, Adam Mickiewicz University Foundation, ul. Rubiez 46, 61-612 Poznan, Poland

<sup>⊥</sup>Faculty of Chemistry, Silesian University of Technology, St. Marcina Strzody 9, 44-100 Gliwice, Poland

<sup>#</sup>Center of Polymer and Carbon Materials, Polish Academy of Sciences, Curie–Skłodowskiej 34, 41-819 Zabrze, Poland

## Supporting Information

**ABSTRACT:** A series of new bis(benzo[*h*]quinolinato) Ir(III) complexes with modified  $\beta$ -ketoiminato ancillary ligands were synthesized, and their electrochemical, photophysical properties were determined with the support of theoretical calculations. Moreover, all the synthesized heteroleptic Ir(III) complexes were examined as dopants of the host–guest type emissive layers in solution-processed phosphorescent organic light emitting diodes (PhOLEDs) of a simple structure. As expected on the basis of voltammetry measurements as well as DFT calculations, all the compounds appeared to be green emitters. Their examination showed that alteration of  $\beta$ -ketoiminato ligand structure causes frontier orbitals' energy levels to be slightly changed, while significantly affecting photoluminescence and electroluminescence efficiencies of iridium phosphors containing these ligands. It was also found that modification of ancillary ligands might enhance charge trapping on the dopant, thus increasing its efficiency, especially in electroluminescence. From among the iridium complexes studied, the compound bearing 1-naphthyl group bonded to the nitrogen atom of the ancillary ligand proved to be the most efficient emitter. The PhOLED fabricated on the basis of this dopant has reached a luminance level of 16000 cd/m<sup>2</sup>, current efficiency close to 12 cd/A, and an external quantum efficiency around 3.2%.



## INTRODUCTION

Intensive research into new organic electroluminescent materials has been ongoing since Tang and Van Slake described the first organic light emitting diodes (OLEDs),<sup>1</sup> and the researchers from the Cambridge University presented the first polymer light emitting diode (PLED).<sup>2</sup> In the first generation of electroluminescent devices, emission occurs mainly from singlet states and is related to the phenomenon of fluorescence. Therefore, according to statistical rules, theoretical internal efficiency of such devices can reach maximally 25%. This limit may be overcome by phosphorescent emitters, for which quantum mechanics selection rules can be broken, and theoretically their emission yield can increase up to 100%.<sup>3</sup> Popular phosphorescent materials are heavy metal complexes bearing organic ligands whose properties result from the presence of strong spin–orbit coupling. The complexes of Pt,

Pd, or Os metals have been studied, but the most examined are Ir(III) derivatives.<sup>4</sup> Popularity of the iridium compounds is related to their intensive phosphorescence, even at room temperature, that might be tuned within the whole visible spectrum depending on the ligand structure modification. It should be emphasized that 2-phenylpyridine was one of the first ligands successfully used in this role and together with benzo[*h*]quinoline gave rise to a group of iridium complexes characterized by very intense green emission, for instance: tris(2-phenylpyridinato)iridium(III) ([Ir(ppy)<sub>3</sub>]) and bis(2-phenylpyridinato-*C*′,*N*)(acetylacetonato)iridium(III) ([Ir(ppy)<sub>2</sub>(acac)]),<sup>5</sup> tris(benzo[*h*]quinolinato-*C*′,*N*′)iridium(III) ([Ir(bzq)<sub>3</sub>]), and bis(2-benzo[*h*]quinolinato-*C*′,*N*′)(acetyl-

Received: September 18, 2019

acetonato)iridium(III) ( $[\text{Ir}(\text{bzq})_2(\text{acac})]$ ).<sup>5</sup> Although the first iridium(III) complexes for OLEDs were developed over 20 years ago, the synthesis and study of new efficient iridium-based emitters is still considered an attractive topic.<sup>4b,6</sup>

In general, emissive materials show higher photoluminescence yield in solution than in solid state (i.e., thin layer) which is related to the self-quenching of excited states. In order to suppress this effect, a host-guest system can be implemented. In such a system, the emitter molecules are dispersed in an active host, e.g. polymeric matrix, that increases the mean distance between two emitter molecules.<sup>7</sup> On the other hand, this approach emphasizes the importance of the intermolecular energy transfer. The yield of energy transfer from the excited states of the matrix to the dopant (by Förster and/or Dexter mechanism) depends on the overlap of the emission spectrum of the host and the absorption spectrum of the guest.<sup>8</sup> Only when this condition is satisfied, a very efficient energy transfer from the host to the guest can take place. Moreover, the emission originating from the guest molecules can be also caused by the direct charge carrier trapping on the dopant.<sup>9</sup> Thus, the host-guest systems can be successfully applied in the form of an efficient emission layer in phosphorescent OLEDs (PhOLEDs).

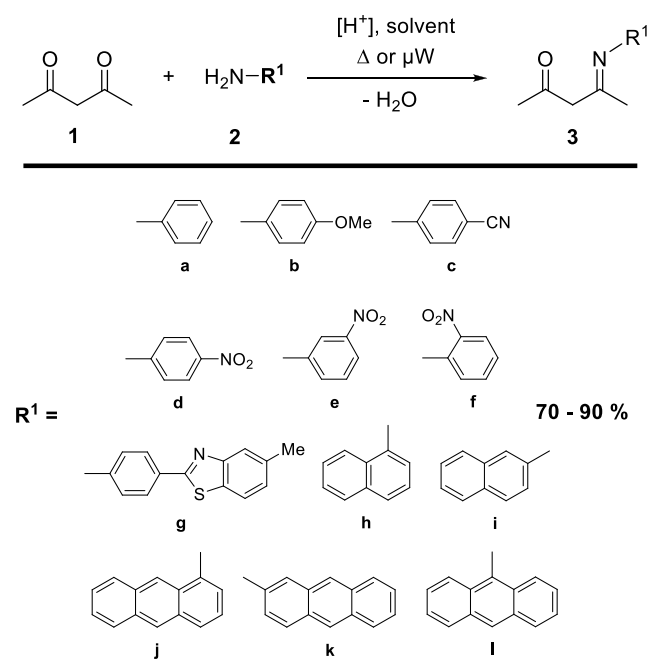
Very recently, we have reported the studies concerning new heteroleptic complexes of the general formula  $[\text{Ir}(\text{bzq})_2(\text{O}\wedge\text{N})]$ , for which we discussed the impact of the number and distribution of fluorine atoms directly bonded to the *N*-aryl moiety ( $=\text{NR}^1$ ) in *N,O*-donating  $\beta$ -ketoiminato ligand ( $\text{RC}(=\text{NR}^1)\text{CH}=\text{C}(\text{O}^-)\text{R}$ ), on the photophysical and emissive properties.<sup>10</sup> We have found that the introduction of fluorine atoms does not significantly modify the optical and electrochemical properties of the iridium complexes, while the electroluminescence performance of PhOLEDs based on them was strongly dependent on the structure of the modified  $\beta$ -ketoiminato ligand. The most promising results were obtained for the Ir complex with 4-fluorophenyl substituent in the ancillary ligand structure. Therefore, as a continuation of our research, we decided to explore *para* substitution effect by investigation of Ir(III) heteroleptic complexes with different substituents in the mentioned position of the phenyl moiety in 4-phenylimino-2-pentanone ancillary ligand. As follows from the available reports on this subject, in particular those by Teets,<sup>11</sup> as well as our recent findings,<sup>10</sup> so far the subjects of studies have been limited to phenyl-based *N*-substituents ( $=\text{NR}^1$ ). Unfortunately, there are no other reports concerning the influence of the higher condensed polycyclic aromatic hydrocarbon used as  $-\text{R}^1$  substituents in *N,O*-donating  $\beta$ -ketoiminato ligand. Therefore, we focused also on the synthesis of 4-arylimino-2-pentanones ( $\text{MeC}(=\text{NR}^1)\text{CH}_2-\text{C}(=\text{O})\text{Me}$ ) equipped with various polycyclic aromatic moieties  $-\text{R}^1$ , which were further employed in the preparation of new  $[\text{Ir}(\text{bzq})_2(\text{MeC}(=\text{NR}^1)\text{CH}=\text{C}(\text{O})\text{Me})]$  type complexes. The modification of  $\beta$ -ketoiminato ancillary ligand allowed determination of the  $=\text{NR}^1$  substitution effect on the emitter photochemical properties. The obtained iridium complexes were applied as dopants in PhOLEDs, whose work parameter analysis allowed identification of the most efficient and promising iridium emitters.

## RESULTS AND DISCUSSION

**Synthesis.** According to recently published protocols,<sup>10</sup> in the initial step a series of 4-arylimino-2-pentanones, bearing aryl substituents of variable stereoelectronic character **3a–l** at

nitrogen atom, were successfully synthesized. Some of the desired derivatives (**3a–f**, **h**, **i**) were prepared by the classical manner, i.e. the refluxing of appropriate amines (**2a–f**, **h**, **i**) with 2,4-pentanedione (*acacH*) in the presence of *p*-toluenesulfonic acid in a benzene environment, using a Dean–Stark apparatus. However, the conversion of more hindered amines (**2g**, **j–l**) required an acceleration with microwave irradiation as a non-classical energy source (Scheme 1). Anyhow, these methods allowed us to obtain  $\beta$ -

Scheme 1. Synthesis of Ancillary Ligands

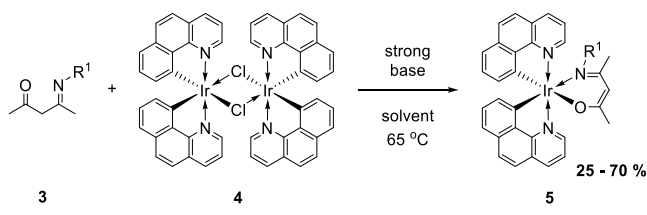


ketoimines equipped with phenyl-based substituents bearing in their structure groups characterized by strong electron withdrawing properties (**3c–f**), including various regioisomers of nitro-substituted derivatives (**3d–f**). Thus, in order to explain the influence of the presence of a strong electron withdrawing group and its position on photophysical properties of final heteroleptic Ir(III) complexes, not only *para*-substituted phenyl  $\beta$ -ketoimines, but also the compounds bearing  $-\text{NO}_2$  group in *meta* and *ortho* positions were synthesized. We assumed that different position of the highly electron withdrawing substituent in the phenyl group could significantly affect the emissive parameters of the target iridium complex, as we have previously described for the phenyl group having one fluorine substituent.<sup>10</sup> Additionally, on the basis of the protocol involving the use of microwaves,<sup>10</sup> 4-arylimino-2-pentanones with selected bulky polycyclic aromatic systems were synthesized (**3g–l**). The purity of all organic materials was confirmed by spectroscopic methods, such  $^1\text{H}$ ,  $^{13}\text{C}$  NMR, HRMS (high resolution mass spectrometry) as well as the structures of three of them (**3d**, **j**, **l**) were solved using X-ray methods.

In the next stage of our synthetic work, previously prepared 4-arylimino-2-pentanones were employed in the preparation of new iridium(III) complexes, according to the earlier described method.<sup>10</sup> However, this time instead of microwaves, a classical source of heat was used. The protocol applied consisted of two successive steps, namely, generation of 4-arylimino-2-pentanonate salt in the reaction of  $\beta$ -ketoimi-

ates **3** with NaH or KH in THF solution and employment of the former for cleavage of binuclear precursor **4** (Scheme 2).

### Scheme 2. Synthesis of Heteroleptic $\beta$ -Ketoiminato Iridium(III) Complexes



However, due to encountered vulnerability of the initial ketoimine to degradation during the deprotonation process, the use of NaO<sup>t</sup>Bu as base in a one-pot protocol was required when using **5b** and **5f**. The applied methodologies made it possible to obtain a series of Ir(III)-based phosphors bearing in their structures various types of ancillary ligands (**5a–l**).

Compounds **5a–l** were obtained with moderate to good yields and characterized by spectroscopic methods. In the <sup>1</sup>H NMR spectra, sets of resonance lines characteristic of protons coming from specific parts of ligands were clearly visible, namely, in the region typical of cyclometalated bzq ligand (9.70–9.00 ppm), methine part of *N,O*-donating ancillary ligand (*c.a.* 5.00 ppm), as well as magnetically and chemically non-equivalent methyl groups of ketoiminato ligand (2.00–1.60 ppm). However, the <sup>1</sup>H NMR spectra of some of the isolated materials, namely **5c**, **5f**, **5i**, **5k**, and **5l** revealed the presence of two isomeric forms. We suppose that the reaction selectivity toward the formation of one isomer depends on properties of aryl substituents bonded to imine nitrogen atom, such as steric hindrance or its orientation relative to the *C,N*-cyclometalated ligands. In our opinion, the presence of *N*-aryl substituents in close proximity of the cyclometalated ligands may induce their intramolecular  $\pi$ – $\pi$  interaction ( $\pi$ -stacking), which might be the driving force for the formation of one of the two possible isomers, as it takes place for complexes **5b**, **5d**, **5g**, **5h**, and **5j**. Heteroleptic octahedral iridium(III) complexes with bidentate ligands may exist in the form of various geometrical isomers, such as *N,N*-*trans-mer*, *cis-fac*, *cis-mer* as well as *C,C*-*trans-mer* and their corresponding enantiomeric forms, as reported for the FIrpic complex.<sup>12</sup> The authors of the cited publication showed that the geometrical isomers do not differ in photophysical properties, thus we decided not to isolate pure isomers but examine their mixtures. Nevertheless, we wanted to determine exactly which of the possible isomers is formed in predominance. Therefore, the structures of five complexes (**5f**, **g**, **i**, **j**, **l**) were determined by X-ray analysis and are discussed in the next paragraph.

**X-Ray Analysis.** X-ray diffraction structural analysis confirmed the obtention of target molecules (Figures 1 and 2 and Figure 23S in the SI). Although the crystal structure of **3d** has been published earlier,<sup>13</sup> for the sake of completeness, we decided to add this structure determination as well. The relevant geometrical parameters are listed in Table 2S (see the SI). In all complexes the Ir atom is six-coordinated in quite a regular octahedral fashion, surrounded by N and O atoms from ketoiminato fragment, and N and C atoms from two benzo[*h*]quinolinato ligands. Table 2S (see the SI) shows that, upon complexation, the C4–N5–C6 angle becomes significantly smaller, while the conformation of the 4-imino-2-

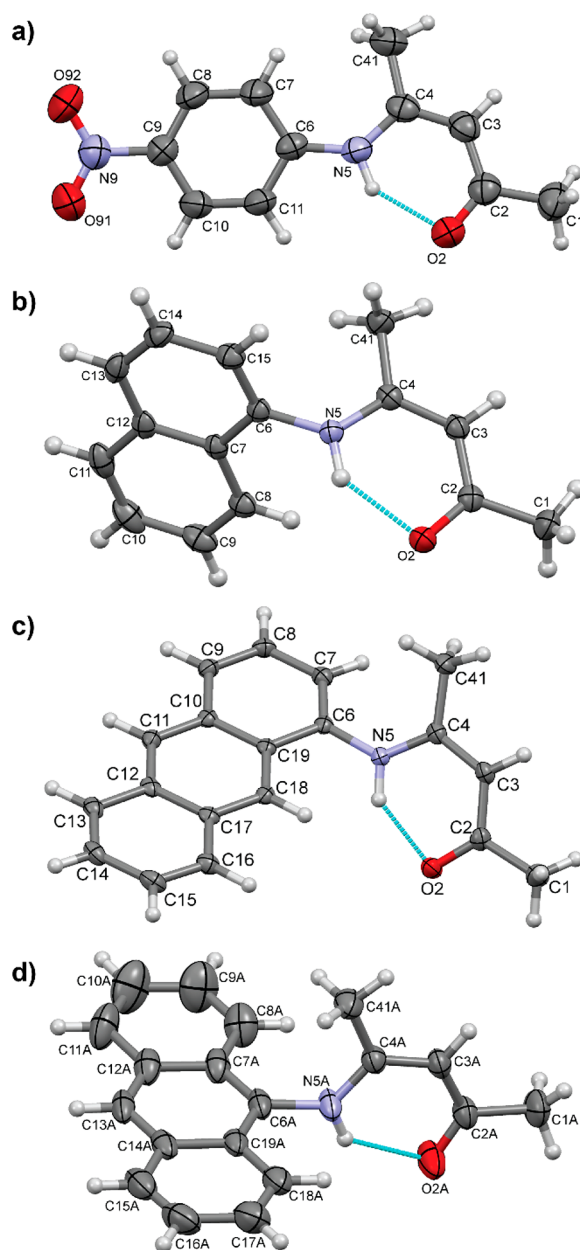


**Figure 1.** Perspective views of ligands: (a) **3d**, (b) **3h**, (c) **3j**, (d) **3l** (molecule A), together with the labeling schemes. Ellipsoids are drawn at the 50% probability level, hydrogen atoms are shown as spheres of arbitrary radii, and intramolecular hydrogen bonds are drawn as dashed blue lines.

pentanone fragment remains stable, although less planar. This observation can be connected with the presence of intramolecular N–H $\cdots$ O hydrogen bonds in free ligand molecules, responsible for planarization (cf. Table 3S, see the SI). What is more, the plane of the aromatic substituent at N5 (Table 2S, the SI) is almost perpendicular to the O=C=C–N plane (Table 2S, see the SI) in the coordinated ligands. The conformations of all complexes, whose structural data are collected, are quite similar. This can be shown by a comparison of the dihedral angles between planar fragments: Ir–ketoiminato cycle, two bzq planes, and substituent at N5. Table 2S (see the SI) lists the appropriate values, and the data can be summarized as follows: (i) the Ir–ketoiminato ring plane is almost perpendicular to all of the other planes, (ii)

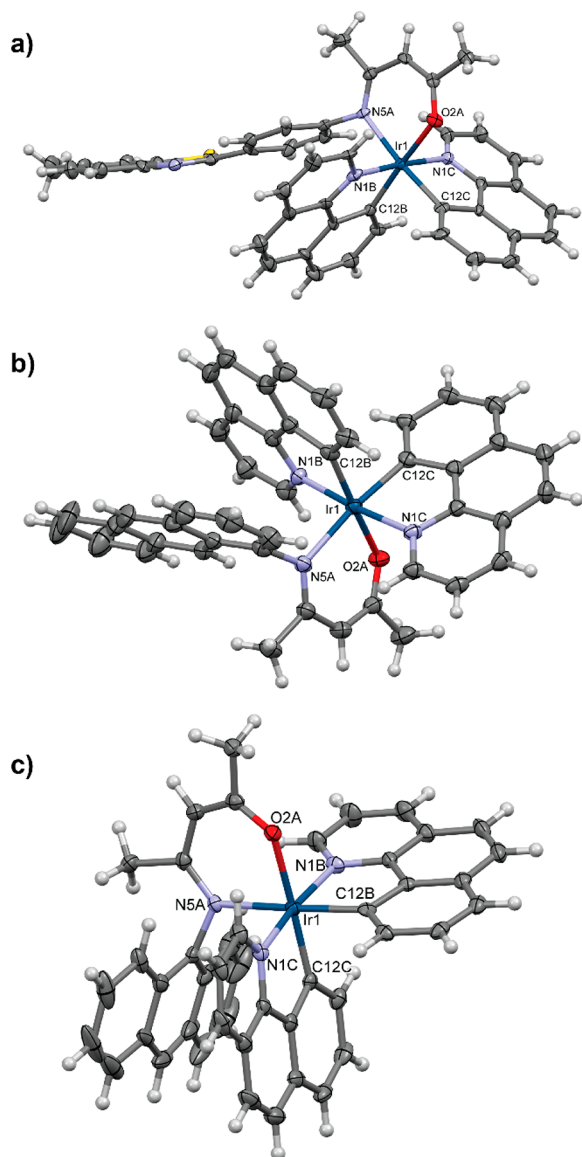


**Figure 2.** Perspective views of iridium complexes: (a) **5g**, (b) **5j**, (c) **5l**. Only Ir and coordinated atoms are labeled, for clarity. Ellipsoids are drawn at the 50% (a and c) and 33% (b) probability level, and hydrogen atoms are shown as spheres of arbitrary radii.

benzo[*h*]quinolinato planes are almost perpendicular to each other, and (iii) the aromatic substituents at NS assume positions close to *gauche* with respect to one benzo[*h*]quinolinato ligand and almost parallel to the other. In all complexes, the tendency toward such a parallel disposition is accompanied by a relatively close interplanar separation (in all cases ca. 3.6–3.7 Å; centroid-to-centroid distances are around 3.8–3.9 Å) which can be connected with the weak intramolecular  $\pi\cdots\pi$  interactions.

The crystal structures are defined mainly by weak dispersive forces. Calculations of intermolecular (molecule-to-molecule) potential using UNI force field<sup>14</sup> indicate that the stabilizing energy is the largest for pairs for which  $\pi\cdots\pi$  (−57.5 kJ/mol for **5l**, −67.0 kJ/mol for **5g**), C–H $\cdots\pi$  (−65.8 kJ/mol for **5j**), C–H $\cdots$ S (−67.0 kJ/mol in **5g**), or C–H $\cdots$ O (−48.1 kJ/mol in **5f**) intermolecular interactions can be found.

Considering the above, it seems that even weak intramolecular  $\pi\cdots\pi$  interactions between the *N*-aryl group and the

*C,N*-cyclometalated bzq ligand might induce the selective formation of only one isomer as it takes place for compounds **5b–d** and **5g–j** (see <sup>1</sup>H NMR spectra in the SI). On the basis of XRD analysis of single crystals obtained from isomerically pure samples **5g** and **5j**, we assume that for the above-mentioned complexes, *N,N-trans-mer* is the most preferred geometric isomer, which is confirmed by spectroscopic studies. This might be supported by the fact that such a configuration of *C,N*-donating ligands around the metal atom is typical of such a binuclear substrate.<sup>15</sup> However, in the case of any disturbances of this type of interactions related to the mutual arrangement of the above-mentioned elements of the complex molecule, e.g. by introduction of a substituent at position 2 relative to the N–C(Aryl) bond (**5f**) or changing the substitution site of the polyaromatic system (**5i**, **5k**, **5l**) (see <sup>1</sup>H NMR spectra in the SI), the formation of another isomer was observed.

**Thermal Analysis.** Thermal decomposition process of all discussed Ir complexes was essentially multimodal with two or three well-pronounced steps observed. The first decomposition step occurred in the range of 250–450 °C, followed by the second one, less pronounced, in the range of 450–650 °C and the third one which could be observed between 650 and 950 °C. Comparing the results of TG analysis presented in Table 1

**Table 1.** Results of TG and DTG Analysis

sample	mass loss temperature [°C]		residue <sup>a</sup> [%]
	<i>T</i> <sub>5%</sub>	<i>T</i> <sub>10%</sub>	
<b>5a</b>	272	333	23.9
<b>5b</b>	300	340	24.3
<b>5c</b>	238	313	26.2
<b>5d</b>	302	343	24.3
<b>5e</b>	278	338	24.4
<b>5f</b>	217	313	23.5
<b>5g</b>	349	376	25.6
<b>5h</b>	233	318	21.7
<b>5i</b>	339	367	23.2
<b>5j</b>	311	358	23.2
<b>5k</b>	313	351	22.6
<b>5l</b>	238	329	21.1

<sup>a</sup>Measured at 990 °C.

as well as TG curves presented in Figures 24S–33S, it can be concluded that the most thermally stable are complexes **5g** and **5b** with the temperatures of 5% mass loss exceeding 230 °C.

Careful analysis of the obtained data leads to the observation that not only the chemical nature of the functional group present in the phenyl ring (see Figure 24S) influence the thermal stability of examined compounds but also its regioisomerism. This phenomenon can be easily observed in the example of TG curves of 4-, 3-, and 2-substituted nitrophenyl **5d**, **5e**, and **5f** derivatives presented in Figure 25S. While only slight differences are observed between the thermograms of **5d** and **5g** isomers, the thermal stability of **5f** is significantly lower, which was revealed by a decrease in the temperatures *T*<sub>5%</sub> and *T*<sub>10%</sub> (see Table 1). The influence of regioisomerism on thermal stability of the studied compounds was also confirmed by the results obtained for 1- and 2-naphthyl (**5h**, **5i**), as well as for 1-, 2-, and 9-anthracenyl (**5j**, **5k**, and **5l**) derivatives TG analysis, presented in Figure 26S and 27S, respectively. Comparing the TG curves of the above-mentioned naphthyl and anthracenyl derivatives with phenyl-

derived complex (**5a**), it is easy to notice that also the number of condensed aromatic rings present in the structure of R substituent unambiguously influences the complex stability (see Figures 30S–33S). Despite the above-mentioned differences in the thermal stability of the investigated samples, the relative residue at 990 °C was similar. The latter was expected as the iridium should be the main component of the pyrolysis residue, and its content in the examined compounds was comparable.

As a conclusion of this paragraph, it might be said that all the complexes exhibited sufficient thermal stability to be applied as potential phosphorescent emitters.<sup>16</sup>

**Electrochemical Properties.** In order to determine electrochemical properties of the studied iridium(III) complexes, in particular their correlation with the structure of  $\beta$ -ketoiminato ligand, cyclic voltammetry measurements were performed. On the basis of the onsets of oxidation and reduction potentials, the electron affinity (EA) and ionization potential (IP) were estimated. The measured curves are shown in Figure 34S (SI). The oxidation onset potentials ( $E_{\text{ox onset}}$ ) of all studied complexes are in the range from 0.12 up to 0.29 V. The oxidation is quasi-reversible and related to the oxidation of Ir(III) to Ir(IV). These results are in good agreement with those reported for the corresponding iridium complexes with  $\beta$ -ketoiminato ligands.<sup>10,11</sup> The incorporation of a methoxy group to the phenyl moiety leads to a slight decrease in  $E_{\text{ox onset}}$  with respect to that of **5a**, while incorporation of nitrile or nitro groups leads to  $E_{\text{ox onset}}$  increase (**5d**, **5e**) or has no effect (**5f**). This is consistent with the electronic effects of these groups, since the methoxy group is electron donating, while nitrile and nitro groups are electron withdrawing. For polycyclic aromatic substituted complexes (**5h–l**), the most intensive influence on  $E_{\text{ox onset}}$  was observed for  $\alpha$ -naphthyl derived complex. As one can see, the measured reduction onset potentials ( $E_{\text{red onset}}$ ) were significantly more varied than  $E_{\text{ox onset}}$ . In general, most of the complexes were characterized with  $E_{\text{red onset}}$  near  $-2.3$  V, while the values reported for methoxy- and nitrile-derived complexes were slightly more positive. However, the most outstanding values were measured for nitro-derived complexes (**5d–f**). The three complexes showed quasi reversible reduction in contrast to the other studied compounds whose reduction was irreversible. These results are similar to those in the other reports concerning iridium complexes equipped with nitro group, in which a drastic change in the reduction potential was also observed.<sup>17</sup>

Electrochemical EA and IP were estimated from  $E_{\text{red onset}}$  and  $E_{\text{ox onset}}$  respectively. EA, which corresponds to the energy level of LUMO (the lowest occupied molecular orbital), was found to be more sensitive toward ancillary ligand chemical modification than IP, corresponding to the HOMO (the highest occupied molecular orbital) energy level. According to Table 2, EA values were within the 2.8–3.4 eV range, while the IP spread was only 0.2 eV. Therefore, the chemical modification had noticeably greater impact on the LUMO energy level. It is worth emphasizing that the complexes equipped with naphthyl or anthracenyl substituents (**5h–l**) were characterized by identical EA and IP values as the reference complex **5a**.

Results of electrochemical measurement show that the incorporation of different electron withdrawing or electron donating groups to  $\beta$ -ketoiminato ligand might lead to a change in their electrochemical properties. Obviously, it is a consequence of electron density shift caused by chemical

Table 2. Electrochemical Properties of Studied Compounds

compound	$E_{\text{red onset}}$ [V]	$E_{\text{ox onset}}$ [V]	$E_{\text{g}}$ [eV]	EA [eV]	IP [eV]
<b>5a</b>	−2.32	0.17	2.49	2.8	5.3
<b>5b</b>	−2.20	0.12	2.32	2.9	5.2
<b>5c</b>	−2.15	0.21	2.36	3.0	5.3
<b>5d</b>	−1.73	0.26	1.99	3.4	5.4
<b>5e</b>	−1.70	0.26	1.96	3.4	5.4
<b>5f</b>	−1.72	0.17	1.89	3.4	5.3
<b>5g</b>	−2.35	0.29	2.64	2.8	5.4
<b>5h</b>	−2.28	0.23	2.51	2.8	5.3
<b>5i</b>	−2.31	0.16	2.47	2.8	5.3
<b>5j</b>	−2.29	0.20	2.49	2.8	5.3
<b>5k</b>	−2.26	0.18	2.44	2.8	5.3
<b>5l</b>	−2.31	0.15	2.46	2.8	5.3

modifications of the studied complexes and, hence, modification of their HOMO and LUMO energy levels. Our attention was drawn by the most outstanding EA change observed for nitro-derived complexes, that must have come from the presence of  $-\text{NO}_2$  groups. Thus, we decided to implement computational chemistry methods in order to explore the electronic structure of these three compounds along with the other complexes, intending to explain the origin of the difference.

**Theoretical Considerations.** As the basis for further theoretical considerations, at first the complexes' geometries were optimized at the B3LYP level without any symmetry constrains. Cartesian coordinates of the ground states ( $S_0$ ) of the complexes are presented in Tables 10S–21S, while the exemplary perspective view of **5f** structure is shown in Figure 3. Table 3 illustrates the parameters of Ir–ligand bond lengths

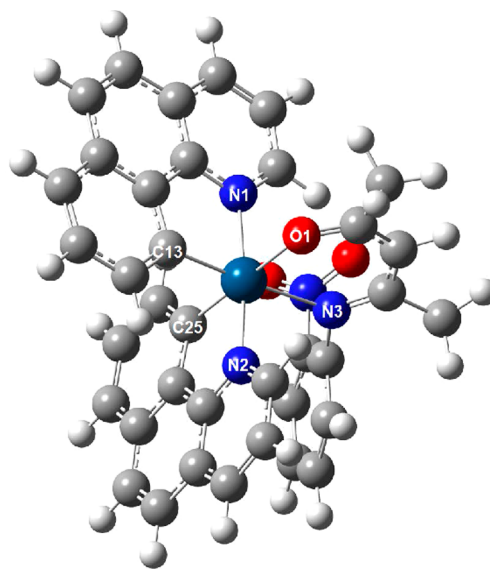


Figure 3. Optimized structure of **5f** in the ground state.

and bond angles *in vacuo* and in the  $\text{C}_6\text{H}_5\text{Cl}$  media, together with the X-ray crystal structure data of **5f**. Due to the  $d^6$  configuration of the Ir(III) ion, all complexes have the expected pseudo-octahedral coordination geometry around the iridium center. As presented in Figure 3 and Table 3, two coordinating nitrogen atoms in the bzq ligands (N(1) and N(2)) are in *trans* positions and the valence angles N(1)–Ir–N(2) are nearly  $180^\circ$ , while the coordinating carbon atoms

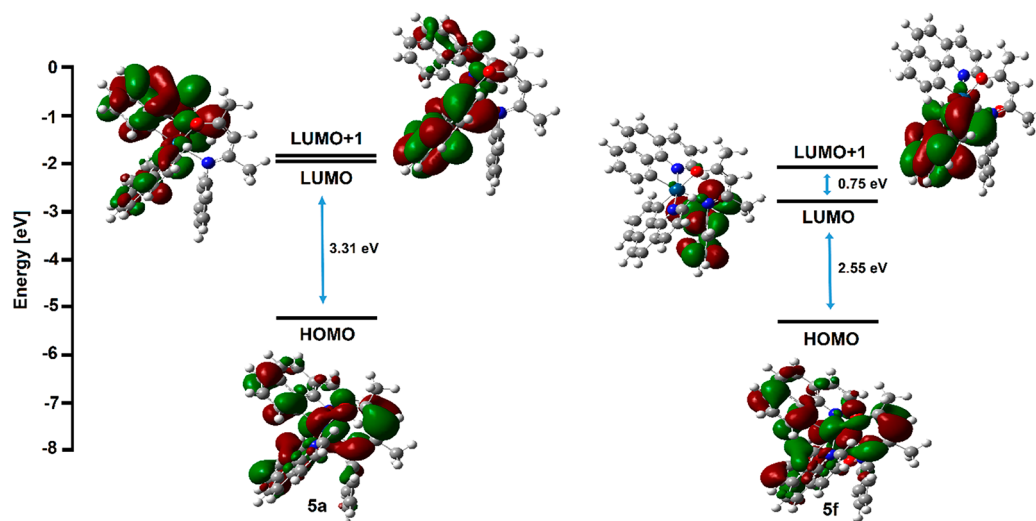
**Table 3.** Comparison of Selected Bond Lengths and Valence Angles from the Optimized Geometries with the Experimental Values for **5f**

	gas	C <sub>6</sub> H <sub>5</sub> Cl	X-ray
Bond Lengths (Å)			
Ir–N1	2.102	2.105	1.946
Ir–N2	2.076	2.080	1.899
Ir–N3	2.265	2.271	2.195
Ir–C13	2.034	2.036	2.034
Ir–C25	2.028	2.029	2.009
Ir–O1	2.180	2.191	2.125
Valence Angles (deg)			
C13–Ir–C25	89.2	88.4	92.5
C13–Ir–N2	93.4	93.6	91.2
C25–Ir–N2	80.9	80.8	81.6
C13–Ir–N1	80.5	80.4	82.7
C25–Ir–N1	98.1	98.0	98.3
N2–Ir–N1	173.8	173.9	173.9
C13–Ir–N3	174.4	174.7	173.8
C25–Ir–N3	95.8	96.2	93.4
N2–Ir–N3	89.9	89.8	91.6
N1–Ir–N3	96.2	96.2	94.5
C13–Ir–O1	89.0	89.5	85.9
C25–Ir–O1	174.8	175.1	177.0
N2–Ir–O1	94.3	94.9	96.0
N1–Ir–O1	86.5	86.0	84.0
N3–Ir–O1	86.2	86.1	88.4

(C(13) and C(25)) are in *cis* positions and the valence angle C(13)–Ir–C(25) is close to 90°. Furthermore, two valence angles between the coordinating atoms from the bzq ligand and the central iridium atom, namely C(13)–Ir–N(1) and C(25)–Ir–N(2) (Table 3 and Figure 3) are nearly identical, ca. 80°. The comparison of the structural parameters calculated in the chlorobenzene environment and *in vacuo* showed that the solvent effects have minor influence on the optimized geometries of these complexes. The calculated Ir–N, Ir–C, and Ir–O bond lengths are slightly longer (up to 0.01 Å) in C<sub>6</sub>H<sub>5</sub>Cl media, while changes in the bond angles are less than 1.0°.

In general, the DFT (density functional theory) calculation results are in reasonable agreement with the X-ray crystal structure data. The deviations measured by the mean unsigned error are 0.08 Å and 2° for bond lengths and valence angles, respectively. The slight discrepancy between the calculated and the measured values is reasonable, because the former results were obtained adopting the complex molecules *in vacuo*, whereas the latter ones were examined in the crystalline state. The above differences of geometrical parameters were indeed expected as B3LYP method overestimates the bond lengths in transition metal complexes.<sup>18</sup>

Spectral properties are strongly dependent on the frontier molecular orbitals' (FMOs) properties. Therefore, DFT calculations were employed to investigate the HOMO and LUMO of the complexes. The molecular orbitals were calculated assuming the optimized geometry of the ground state. For all complexes, the energy gaps between the HOMO and LUMO were correlated with their experimental values obtained by cyclic voltammetry measurements. In this study, apart from B3LYP, other commonly used functionals, namely M06 and WB97XD with basis set composed of 6-311++G(d,p) for H, C, N, and O and SDD for Ir atom, were tested to obtain the best possible correlation with experimental values. Because the geometries optimized with B3LYP were comparable to those obtained from the experimental XRD results, we initially adopted this approach in our studies. The linear regression coefficient determined, characterizing the strength of the correlation between the theoretical energies and electrochemical data, was 0.86 (Figure S35 SI). From among the other tested functionals, B3LYP was characterized by the best correlation between experimental results and allowed us to explain the unusually low bandgap for **5d–f**; thus, it was chosen for further considerations. This choice was also supported by the fact that B3LYP functional is applicable for prediction with good accuracy of the trend of structural changes effect on the electronic structure of the modified compound with respect to that of the unmodified one.<sup>19</sup> The exemplary HOMO and LUMO contours and HOMO–LUMO energy gaps of the studied complexes are presented in Figure 4, while the full set of the numerical values of orbital distributions are compiled in Table 9S (see the SI).

**Figure 4.** Frontier molecular orbital diagrams of complexes **5a** and **5f** computed at the B3LYP/SDD/6-311++G(d,p) level of theory.

As usually observed for cyclometalated cationic iridium(III) complexes,<sup>18,19</sup> the iridium atom brings a significant contribution to HOMO, while being much less involved in LUMO. This fact indicates that HOMO–LUMO transition should be characterized by strong MLCT (metal to ligand charge transfer) character. Therefore, the HOMOs are localized on both types of ligands, but their distribution is limited to the *N,O*-donating atoms of the  $\beta$ -ketoiminato ligand and is also spread over the whole bzq ligands, with slight shift of electron density toward the *C*-donating part of bzq. On the contrary, the LUMOs are almost totally present on cyclometalating ligands (except **5d–f**) with less than 5% contribution of the Ir atom. It is worth noting that due to the lack of symmetry constraint in the calculated structures, the two bzq ligands are inequivalent, so their LUMOs are split into two subsequent levels (e.g., LUMO and LUMO + 1) that are very close in energy. However, for complexes **5d–f** equipped with a nitro group, the LUMOs are mainly located on the ancillary ligand, in particular its nitrophenyl moiety, while the successive unoccupied molecular orbitals LUMO + 1 and LUMO + 2 primarily originate from the cyclometalating ligands (see Table 9S in the SI). According to Table 6S, the bandgap values calculated for **5a–c** and **5g–i** are very close, the spread is 0.21 eV, while the respective electrochemical bandgap spread is 0.32 eV. The calculated bandgap spread for **5d–f** is 0.11 eV, while electrochemically determined bandgaps are within 0.1 eV range. This indicates that the electrochemical data and theoretical predictions are well correlated and show that the mentioned complexes should exhibit similar properties related to the bandgap values within the above-specified groups, despite the fact that their LUMO levels are overestimated. Additionally, the calculated **5d–f** bandgaps are lower than the value obtained for the reference **5a** by about 0.8 eV for B3LYP functional (Table 6S). The respective electrochemically determined difference is in the 0.5–0.6 eV range, which indicates good reproducibility of the experimental data by theory. Interestingly, if one calculates HOMO and LUMO + 1 energy level differences for **5d–f**, they will obtain a value close to the calculated HOMO–LUMO bandgap of **5a**. Considering the above, the DFT calculations reproduced the trends observed in electrochemical measurements, confirming that incorporation of  $-\text{NO}_2$  groups into the ancillary ligand structure is associated with the insertion of its own lowest unoccupied level between the original HOMO and LUMO levels of the unmodified reference complex **5a** (see Figure 4). Therefore, it supports our supposition that  $E_{\text{red onset}}$  decreases for **5d–f** complexes relative to the other complexes which originates from the reduction of the nitro group itself. This conclusion is very important since it indicates that the electrochemically determined bandgaps for these three complexes are flawed. The correlation of electronic structure with photophysical properties of the complexes is further discussed in the following sections.

**Photophysical Properties.** Absorption spectra of the studied complexes **5a–5l** in chlorobenzene under ambient conditions are presented in Figure 5. The strong spin–orbit coupling of iridium atom makes the formally forbidden triplet metal–ligand charge transfer transitions ( $^3\text{MLCT}$ ) possible, and for the examined complexes, they are observed as long-wavelength absorption bands in the range of 440–550 nm. Generally, the bands located around 400 nm can be assigned to the higher extinction singlet  $^1\text{MLCT}$ , and the bands falling in the short-wavelength range (below 400 nm), to  $\pi-\pi^*$  ligand

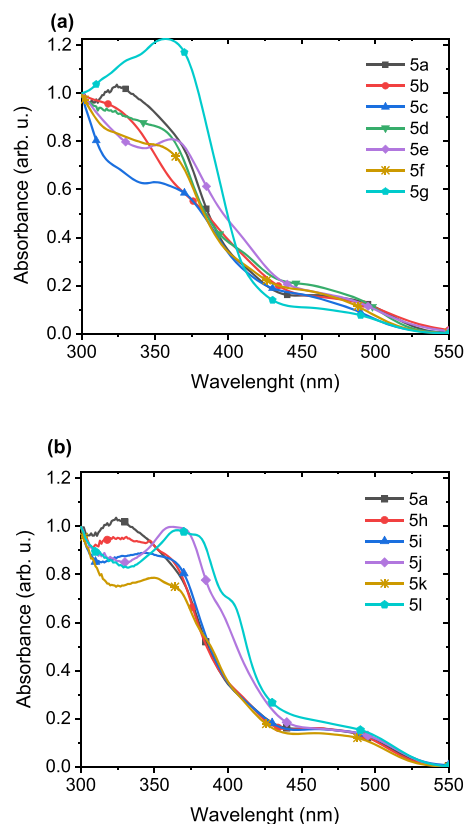


**Figure 5.** Normalized absorption spectra of the investigated complexes in chlorobenzene: **5a–5g** (a) and **5h–5l** compared with **5a** (b).

centered ( $^1\text{LC}$ ) transitions. However, the exact assignment of the lowest energy states may be inaccurate, because it is generally known that they can be a mixture of  $^3\text{LC}$ ,  $^3\text{MLCT}$ , and  $^1\text{MLCT}$ .<sup>4b</sup> The fact that for tris(benzo[*h*]quinolino)-iridium(III) complex ( $[\text{Ir}(\text{bzq})_3]$ ) the absorption bands in the 370 nm region were assigned to  $^1\text{MLCT}$  states might support our interpretation.<sup>20</sup>

As one can see, the performed modifications of  $\beta$ -ketoiminato ancillary ligand structure did not affect significantly the absorption spectra of the studied complexes. Nonetheless, the absorption spectra of the complexes equipped with polycyclic aromatic substituents, especially anthracenyl, differ mostly in the range of  $^1\text{MLCT/LC}$  transitions. Interestingly, the change in anthracenyl regio-substitution from position 2 (**5k**) to 1 or 9 (**5j**, **5l** respectively) resulted in alteration in the probability of these transitions. The bands located around 400 nm are more pronounced for **5j** and **5l** complexes, and the most intense bands (350–380 nm) are slightly red-shifted in comparison to the corresponding signals in the spectra of **5a**, **5h**, **5i**, and **5k**. Interestingly, the absorption onset for **5d–5e** is similar to those of the other complexes and no additional low-energy absorption bands were observed for them. This fact is in contrast to the electrochemically determined energy levels, which suggests a significant decrease in the bandgaps for the nitro-substituted complexes. This indicates that the excitation from HOMO to LUMO levels are not preferable for them. Therefore, it can be supposed that the observed lowest in energy transitions involve the central atom and bzq ligands (corresponding to HOMO  $\rightarrow$  LUMO+1 transition). The reason for that might be the

location of LUMO on the nitrophenyl moiety of ancillary ligand, which hampers the electron transition from HOMO mostly located on bzq ligands, due to very poor overlapping of the orbitals.

Normalized photoluminescence (PL) spectra of the studied complexes in chlorobenzene are shown in Figure 6. Excitation

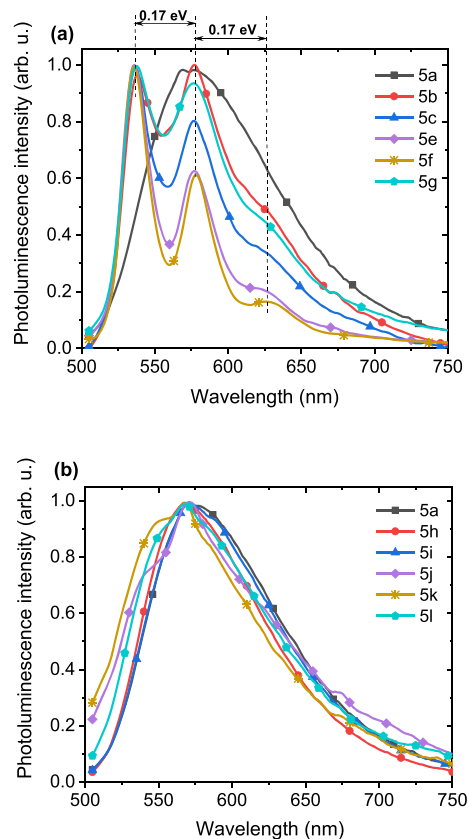


**Figure 6.** Normalized photoluminescence spectra of the investigated complexes in chlorobenzene ( $\lambda_{\text{ex}} = 485 \text{ nm}$ ): **5a–5g** (a) and **5h–5l** compared with **5a** (b).

at 485 nm, corresponding to the  $^3\text{MLCT}$  transition of the complexes, resulted in a broad emission band in the range of 500–750 nm with a maximum at  $\sim 570 \text{ nm}$  for the complexes with phenyl, naphthyl, and anthracenyl substituents (**5a** and **5h–5l**). All other complexes (**5b–5g**) showed a structured emission with narrow bands located at  $\sim 538$ ,  $\sim 577$ , and  $\sim 628 \text{ nm}$ . The most structured emission spectrum was observed for complexes **5e** and **5f**, equipped with  $-\text{NO}_2$  groups. Nonetheless, the emission spectra of the complex with  $-\text{NO}_2$  groups in the *para* position (**5d**) revealed its instability and thus, it was not further examined (see Figure 36S in the SI). As one can see, the most pronounced structure is observed for the complexes bearing electron withdrawing substituents (e.g.,  $-\text{NO}_2$ ,  $-\text{CN}$ ) and less distinct bands are noticed when the electron donating groups (e.g.,  $-\text{OCH}_3$ ,  $-\text{Ph}$ ) are present in the ancillary ligand structure. The structured emission spectra of transition metal complexes often indicate a large contribution of LC in the emissive excited states.<sup>21</sup> Additionally, for the complexes with electron withdrawing group, the most intense is the 0–0 transition that changes a little bit the color of the emitted light and suggests small geometry changes during excitation and relaxation.

Complexes from the first group (**5b–5g**) exhibited the structured emission which was a mirror image of the excitation spectra (compare Figures 6a and 7), as relative intensities of

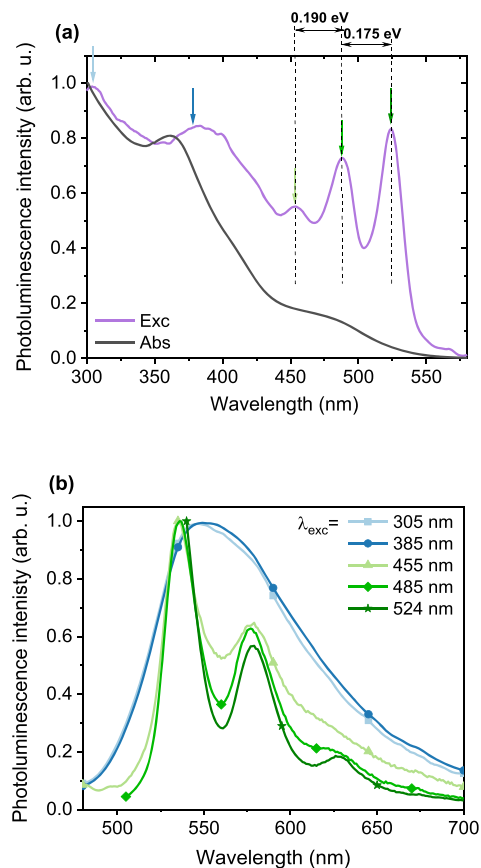


**Figure 7.** (a) Normalized photoluminescence excitation and absorption spectra of **5e** in chlorobenzene. (b) Normalized photoluminescence spectra of **5e** in chlorobenzene, measured at different excitation wavelengths.

the vibrational peaks in the emission correlated with the excitation spectra (see Figure 37S in the SI for a full data set). Considering the spectra recorded for the nitro-derived complexes **5e** and **5f**, the emission structure is the most visible and the probability of higher energy transition relative to the other bands is higher. For many common fluorophores, the vibrational energy levels spacing is similar for the ground and excited states, which results in the emission spectrum that strongly resembles the mirror image of the absorption spectrum. However, for our complexes, the vibrational mirror image is only visible in the excitation spectra and no structure is observed in the absorption spectra. It may suggest that these two spectra have different excited-state origins. It is supposed that the first absorption band reflects a combination of different transitions to MLCT states, whereas the excitation spectrum comes from the specific state responsible for the emission. In general, MLCT transitions are coupled to low energy vibrations and are more influenced by the molecule's environment, thus the absorption bands should reveal more inhomogeneous broadening with increasing degree of MLCT character. As shown for **5e** (Figure 7), when its molecule was excited at the lowest energy absorption bands observed in the excitation spectra, a structured emission spectrum in photoluminescence was recorded. Nevertheless, when higher energy

was supplied to the molecule, a broad and structureless emission spectrum was found. Usually, the structureless emission spectrum is assigned to the emission from MLCT states, whereas the structured emission indicates that LC emissive excited states play a crucial role in generation of visible light. Therefore, the probable explanation of this behavior could be that upon tuning the excitation energy, the emission from different close lying excited states is observed. However, in order to examine this phenomenon, additional experiments are needed. The strong excitation wavelength dependency of emission have been reported by Hsu et al. for osmium(II) and silver(I) complexes<sup>22</sup> in which the phosphorescence/fluorescence intensity ratio is enhanced when the excitation energy is increased.

Additionally, LC transitions are characterized with higher energy than MLCT transitions.<sup>23</sup> However, our results obtained for the studied iridium complexes suggests almost the same energy for both transitions and a strong mixing of LC and MLCT. Since the structured emission was observed only for the complexes bearing phenyl-based ketoimine ancillary ligands, we expected that this phenomenon would be connected with the presence of this moiety. Surprisingly, with the higher energy applied for excitation of **5e** and **5f**, their emission spectra were almost the same as those of the other compounds. Once again, it proved that the electron transitions involving nitrophenyl moiety are not preferable and rather Ir-bzq are engaged, which correspond to HOMO–LUMO+1 and HOMO–LUMO+2 transitions. This explanation was further supported by the results of electroluminescence studies.

[Ir(bzq)<sub>3</sub>] is classified as a complex whose emission originates from the <sup>3</sup>MLCT state.<sup>20</sup> A comparison of its emissive properties with the results reported here suggest that  $\beta$ -ketoiminato ancillary ligand plays rather a marginal role in the emission processes that originates mainly from the states in which bzq and iridium are mostly involved. As a consequence, the observed structured photoluminescence spectrum can correspond to the vibronic–sublevel, especially for the electron transition between the orbitals localized mostly on the ligand, when the electronic–vibronic coupling occurs and/or for low energy metal–ligand vibrations, when the metal participation in the electronic state increases. Since electron transitions are much faster than nuclear oscillations, the structured spectra should be observed when a small molecular geometry change takes place in the excited state. The latter was confirmed previously on the basis of the intensity of 0–0 transition. Therefore, taking into account the above considerations, it can be concluded that substitution of *N*-donating atom in the  $\beta$ -ketoiminato with various aryl groups affects only the LC/MLCT excited states contribution to the total emission, while all the studied [Ir(bzq)<sub>2</sub>(N $\wedge$ O)] complexes exhibit green emission in the same range. Therefore, it should be expected that the modification of ancillary ligand should influence the luminescence performance, since the emission from the <sup>3</sup>MLCT state is expected to be more efficient, but this will not tune the emitted wavelength. Driven by this conclusion, we wanted to examine if the structured emission would occur in photo- and electroluminescence in the solid state.

**Photoluminescence of PhOLED Active Layers.** In order to avoid the concentration induced emission quenching, for which Ir(III) complexes are known,<sup>24</sup> the host–guest systems are commonly used as an active layer, which means that the emitter is homogeneously dispersed in a polymer matrix. In this work, we used a well-known ambipolar matrix, composed

of poly(*N*-vinylcarbazole) (PVK) and 2-(4-*tert*-butylphenyl)-5-(4-biphenyl)-1,3,4-oxadiazole (PBD), providing hole and electron transport, respectively. The PVK/PBD mixture was selected as a host material due to its wide energy gap in accordance with the general rule that the emitter energy gap should be localized between HOMO and LUMO levels of the matrix to ensure good energy transfer of the excitons from the matrix to the emitter molecules.

The PL spectra of thin PVK/PBD films doped with 1 wt % of the studied emitters upon excitation with the wavelength corresponding to the lowest absorption band of the PVK/PBD matrix ( $\lambda_{\text{ex}} = 340$  nm) are presented in Figure 8. All tested

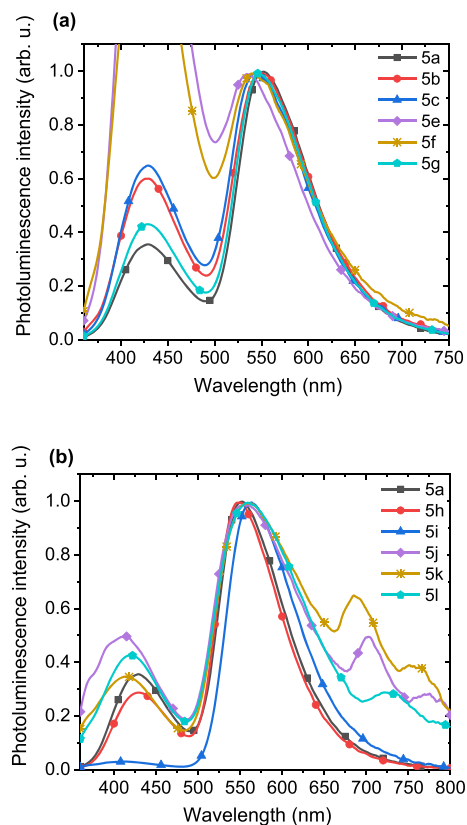


**Figure 8.** Normalized photoluminescence spectra of thin layers of the PVK/PBD blend doped with 1 wt % of emitter molecules: **5a–5g** (a), and **5h–5l** compared with **5a** (b). Excitation wavelength was 340 nm, that corresponds to first absorption band of PVK/PBD matrix.

layers showed the emission related to the phosphorescent dopants as well as host component ( $\lambda_{\text{max}} \sim 430$  nm), originating from singlet exciplexes formed between carbazole moieties and oxadiazole molecules. A contribution of the matrix emission indicates incomplete energy transfer from the matrix to the emitters. The best energy transfer was observed for naphthyl–derived complex (**5i**), whereas the worst efficiency of this process was noted for the complexes characterized by structured emission spectra in solution (primarily **5e**, **5f**). The main photoluminescence bands are generally similar to those detected for the emitters in solution upon high energy excitation. For the neat films, the emission distribution is broadened and less structured, thus indicating that mostly MLCT energy states are responsible for the emission in the examined host–guest systems. Efficiency of such an energy transfer influences the photoluminescence

Table 4. Parameters of PhOLEDs Based on PVK/PBD Layers Doped with 1 wt % of All Tested Ir Complexes

compound	$\lambda_{EL}$ [nm]	$L_{max}$ [cd/m <sup>2</sup> ]	$\eta_{max}$ [cd/A]	EQE [%]	$\lambda_{PLfilm}$ [nm]	QY <sub>film</sub> [%]
5a	559	9 500	9.1	2.71	552	15
5b	565	1400	2.6	0.83	548	8
5c	559	600	1.5	0.48	545	9
5e	567	180	0.2	0.07	534	2
5f	563	580	0.3	0.10	540	2
5g	559	4200	3.8	1.13	548	12
5h	556	15700	12.3	3.20	549	18
5i	569	5500	4.2	1.45	563	4
5j	587, 715	50	0.02	0.01	554, 703, 775	<1
5k	625, 697, 765	100	0.06	0.03	561, 685, 753	<1
5l	575, 740	70	0.02	0.02	559, 723	<1

quantum yield (QY), which was up to 18% for the investigated layers (Table 4).

The emission spectra of thin layers doped with anthracenyl substituted complexes (5j–5l) showed additional low energy bands (680–800 nm) that were not visible in the spectra recorded in solution. The presence of these bands is most likely related to the anthracenyl degradation products. These complexes exhibited poor emissive properties (QY < 1%, Table 4), as well as low stability of emissive states that was also observed in further electroluminescence studies. Additionally, incorporation of 5j–5l complexes resulted in a hypsochromic shift of the matrix emission as presented in Figure 8b. It can be attributed to the disruption of exciplex formation between carbazole moieties from PVK and oxadiazole molecules. Therefore, 5j–5l complexes are not good candidates for efficient emitters in the PVK/PBD matrix, even though their energy transfer was acceptable.

Dominant contribution to the emission of dopant introduced to the layers may originate from long-range Förster and/or from short-range Dexter energy transfer. The Dexter mechanism is less likely because of low emitter concentration. However, the exciton diffusion can enhance both paths of energy transfer. Both mechanisms can operate efficiently only when the emission spectrum of the donor and the absorption spectrum of the acceptor overlap considerably. All the studied complexes are characterized by a good spectral overlap of their MLCT absorption bands with the matrix emission spectrum, as shown in Figure 9, for exemplary 5a and 5h–5i complexes. In the whole group of tested compounds, emitter 5i stands out in the energy transfer efficiency since only a small contribution of

its emission originated from the matrix is visible in the film PL spectrum. However, the photoluminescence QY of this compound in thin film was very low (4%, Table 4). The opposite relationship was observed for 5g, for which the energy transfer was much less effective, but the compound showed higher QY. Furthermore, 5h was characterized with the best quantum yield (18%), despite showing noticeable contribution of matrix emission in the photoluminescence spectrum. These observations indicate that aryl-substitution of  $\beta$ -ketoiminato ancillary ligand can tune photoluminescence efficiency of the complexes in a way not fully understood. Nevertheless, the confirmed spectral overlap of the complex absorption and the matrix emission was a good premise to examine the efficiency of energy transfer in electroluminescence studies.

**Electroluminescent Properties.** The electroluminescence properties of the iridium complexes were tested in one of the simplest PhOLED structure. The devices with a hole injection layer (HIL) and an emissive layer were produced by a spin-coating technique. Such a simple construction of the device is preferable for manufacturing by economical wet printing techniques. Additionally, this minimalistic approach is an easy screening procedure for emitters' electroluminescent properties. The emissive layers were based on PVK/PBD matrix systems as used in photoluminescence studies. It should be noted that a PVK/PBD blend with a 7:3 weight ratio is characterized by balanced charge transport properties, which is a basic requirement for efficient OLEDs.

Electroluminescence (EL) spectra recorded for the devices based on the investigated emitters are presented in Figure 10. The EL spectra obtained for PhOLEDs doped with emitters 5a–5i were very similar to the PL spectra in thin films. The maxima of emission were in the range of 555–570 nm, with one exception, and were only slightly red-shifted in relation to the PL spectra (compare Figures 8 and 10). It should be emphasized that the matrix emission disappeared in the EL spectra, even when it was predominant in PL of thin films (for complexes 5e and 5f). The lack of emission from the matrix in the EL spectra suggests a strong contribution of the charge trapping process in EL phenomenon, which can promote formation of excitons on the dopant molecules.

Similarly to the PL spectra, the EL spectra of PhOLEDs doped with emitters 5j–5l showed long-wavelength bands in addition to the desired <sup>3</sup>MLCT bands. For the PhOLED created on the basis of 5k, this red emission even dominated. During prolonged measurements of these OLED emissions, we observed that the contribution of long-wavelength bands changed irreversibly along with the device operation time (see Figure 38S in the SI). Therefore, it can be concluded that the

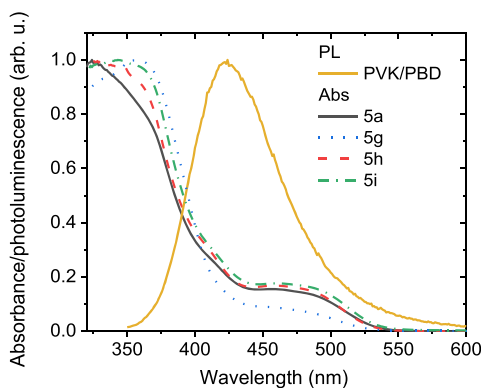
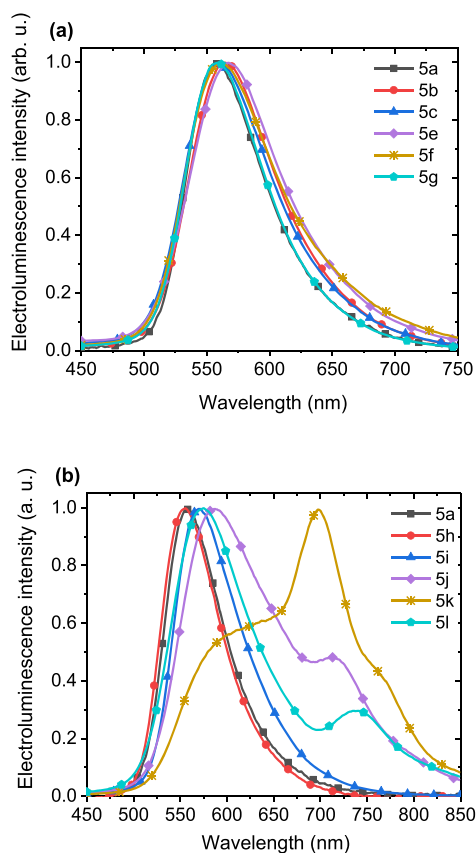


Figure 9. Normalized absorption spectra of four selected compounds (5a, 5g, 5h, 5i) in chlorobenzene solutions and normalized photoluminescence spectra of neat PVK/PBD blend.



**Figure 10.** Normalized electroluminescence spectra of PhOLEDs based on PVK/PBD doped with 1 wt % of the investigated emitter molecules: **5a–5g** (a) and **5h–5l** compared with **5a** (b).

complexes with the anthracenyl substituent (**5j–5l**) are unstable. This indicates that the degradation process of anthracenyl groups may occur during the radiative excitation and can be reinforced during operation of the device. Such a scenario is possible because the degradation might be caused, e.g., by trace amounts of oxygen molecules embedded in the bulk of the emissive layer, despite their production in a nitrogen atmosphere.

Current density–voltage ( $J$ – $V$ ) and luminance–voltage ( $L$ – $V$ ) characteristics of the best performing PhOLEDs, based on **5a** and **5h** emitters, are shown in **Figure 11**. These plots represent typical PhOLED characteristics in the range up to 16

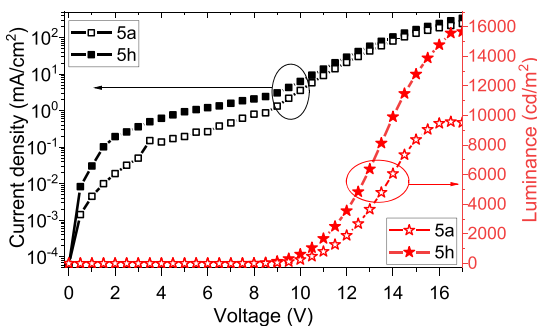


**Figure 11.** Current density–luminance–voltage ( $J$ – $L$ – $V$ ) characteristics of PhOLEDs with emitting layer made of PVK/PBD doped with 1 wt % of emitter molecules: **5a** (empty symbols) and **5h** (full symbols).

V. The obtained luminance values were  $\sim 9500$  and  $\sim 16000$   $\text{cd}/\text{m}^2$  at 16 V for **5a** and **5h** based PhOLEDs, respectively. The turn-on voltage (the voltage value at which the luminance reaches 1  $\text{cd}/\text{m}^2$ ) was around 7 V. Although the **5h**-based PhOLED was characterized by a greater leakage of current; nevertheless, the maximum luminance was higher when compared to the system made with the use of **5a**. In **Figure 12**, the current efficiencies are plotted versus luminance for the

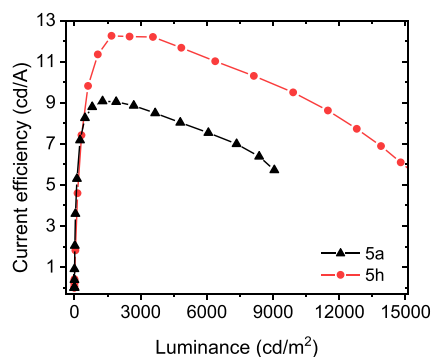


**Figure 12.** Current efficiency–luminance dependencies of PhOLEDs with emitting layer made of PVK/PBD doped with 1 wt % of **5a** and **5h** complexes.

tested devices. The highest value (over 12  $\text{cd}/\text{A}$ ) was obtained for PhOLED with **5h** emitter, derived with a 1-naphthyl substituent. This result correlates well with the fact that the highest photoluminescence  $QY$  was measured for thin films with this dopant (**Table 4**). Moreover, measured current efficiency was relatively stable in the wide luminance range (1500–4000  $\text{cd}/\text{m}^2$ ).

A comparison of the parameters determined for all tested devices and their emissive layers is shown in **Table 4**. It should be emphasized that the best devices exhibited good parameters, considering that the diodes had such a simple structure and were produced using solution methods. OLEDs of similar structure, based on  $[\text{Ir}(\text{bzq})_2(\text{acac})]$ , exhibited the maximum current efficiency of 4.2  $\text{cd}/\text{A}$ .<sup>25</sup> Therefore, the obtained current efficiencies of 9.5 and 12.0  $\text{cd}/\text{A}$  for **5a** and **5h** can be considered to be quite high. Of course, further optimization of the devices' structure by incorporation of additional layers should lead to PhOLEDs of better performance.<sup>26</sup>

The devices that exhibited the best EQE were those with **5a**, **b** and **5g–i** phosphorescent dopants (**Table 4**). As one can see from a comparison of  $QY_{\text{film}}$  and EQE, they correlate well for all complexes with the exception of **5i**. This deviation might be related to a noticeable impact of the exciton energy transfer on the device performance. Considering the above, it seems that the best external efficiencies were obtained for the emitters equipped with unmodified aromatic moieties (**5a** and **5g–i**) and electron-donating methoxy group (**5b**), all rich in electrons. The very low performance of anthracenyl-derived complexes (**5j–k**) might deny it at a first glance, but their poor stability in electroluminescence should be kept in mind. Taking into account the above-mentioned details, it is clear that their efficiency might be suppressed by their unexpected instability. In this way, we proved that  $\beta$ -ketoiminato ligands affect the photophysical properties of the examined complexes, in particular luminescence efficiency, although they do not tune the maximum emission wavelength.

It is known that the performance of PhOLEDs strongly depends on the concentration of emitter in the active layer. After screening all the emitters as dopants for OLEDs at 1 wt %, we decided to optimize the dopant concentration for the complex with the best-performance, i.e. **5h**. This emitter was chosen *inter alia* because of its highest quantum photoluminescence efficiency (18%). Furthermore, the devices based on it exhibited the highest luminance and current efficiency from among the tested PhOLEDs. To determine the optimal dopant concentration, a series of devices with different emitter content in the PVK/PBD matrix were prepared (from 0.5 to 7.0 wt %). The observed maximum luminance values (at 17 V) were in the range from  $\sim 4000$   $\text{cd/m}^2$  (for 7 wt %) to  $\sim 16000$   $\text{cd/m}^2$  (for 1 wt %). The maximum value of external quantum efficiency (EQE  $\sim 3.2\%$ ) was obtained for the devices with 1 wt % emitter additive. A little bit lower value, but with slower reduction of the efficiency with the increase in current density, was observed for the diodes with 2 wt % emitter content (Figure 13). Therefore, it can be assumed that the optimal

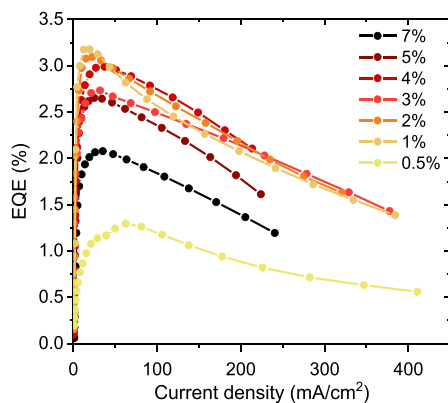


**Figure 13.** External quantum efficiency–current density dependencies of PhOLEDs with emitting layer made of PVK/PBD doped with different concentrations (from 0.5 to 7 wt %) of **5h** emitter.

emitter content for such PhOLEDs ranges between 1 and 2 wt %. Higher concentration may result in the emitter molecules aggregation process resulting in quenching of emissive states that is a common phenomenon observed in guest–host systems. This might be the reason for the decrease in EQE with increasing emitter concentration from 4 to 7 wt % in the examined case.

In order to compare the energy transfer efficiency in electro- and photoluminescence, the same amounts of **5h** dopant were used in both experiments. The obtained normalized PL spectra are presented in Figure 14. As one can see, the contribution of matrix emission decreases as the dopant concentration increases. However, even for 7 wt % emitter additive, a small emission from the matrix exciplexes was observed, so the energy transfer was still incomplete. It strongly contrasts with the electroluminescence spectra, in which almost complete quenching of PVK/PBD emission was observed for the lowest examined concentration (0.5 wt %) of emitter **5h** (see Figure 39S in the SI). As mentioned above, these results suggest that charge carrier trapping processes play an important role in the electroluminescence phenomenon. EL spectra do not change noticeably with the concentration increase and only a slight shift of the band maximum was observed from 557 nm (0.5 wt %) to 560 nm (7 wt %) nm. In the dopant concentration–photoluminescence studies, a slightly bigger redshift from 547

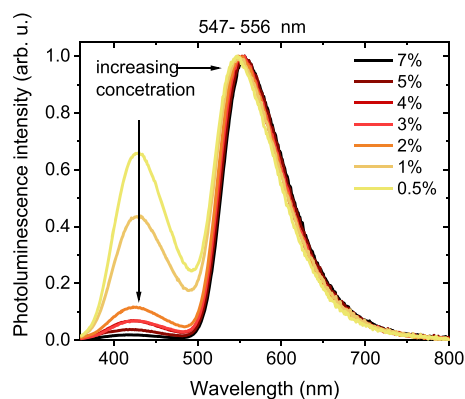


**Figure 14.** Normalized photoluminescence spectra of emissive layers based on PVK/PBD doped with **5h** in different concentrations (from 0.5 to 7 wt %). The excitation wavelength, corresponding to first absorption band of PVK/PBD matrix, was 340 nm.

nm (0.5 wt %) to 556 nm (7 wt %) was observed, suggesting stronger intermolecular interactions. This is a normal consequence of increasing concentration since it should also reduce the mean distance between emitter's molecules in the emissive layer. It is worth noting that this phenomenon is more visible in photoluminescence and less in electroluminescence. Nevertheless, it is undoubtedly clear that the lower dopant concentration gave better results in OLEDs.

As mentioned above, the charge carrier trapping might play an important role in electroluminescence, therefore this phenomenon was further explored by spectrally resolved thermoluminescence (SRTL) studies in the range of 20–300 K. In recent years, it has been proved that guest and matrix molecules compete in charge carriers trapping in emissive layers based on host–guest systems.<sup>9b,27</sup> To maximize the emitter efficiency, this balance should be shifted toward efficient formation of excitons on guest molecules and quenching of host emission, even for the systems with minor content of the emitter molecules in the matrix.

The SRTL results for the neat PVK/PBD and for the PVK/PBD matrix doped with 1 wt % of **5h** are shown in Figure 15. A comparison of the TL maps showed that doping of **5h** into the PVK/PBD matrix results in a change in the emitted light range. The spectrally resolved luminescence (SRL) recorded close to the TL maximum (115 K) revealed that the emission occurs in the range of 490–730 nm with one very broad band with a maximum at 565 nm (see Figure 15c, red dashed line) which does not change its position with temperature (see Figure 15a). For the neat PVK/PBD matrix (see Figure 15c, blue solid line), the emission occurred in the broader range of 390 to 750 nm. One can see two separated emission bands: a dominant one with a maximum at 550 nm and the second one with a maximum at 450 nm. Both emission bands from the PVK/PBD blend are attributed to the exciplexes formed between carbazolyl group and PBD molecule. The dominant band originates from the triplet exciplexes, and the minor one can be related to the singlet exciplexes and/or monomeric triplet states of carbazolyl groups.<sup>27</sup> However, the identification of the radiative recombination active center in the doped matrix is problematic because the dominant emission band of the matrix (550 nm) is close to the emission originating from the iridium complex molecules (565 nm). Nevertheless, comparing both spectra, one can see that the spectrum of the matrix doped with **5h** is more intensive and has no short-

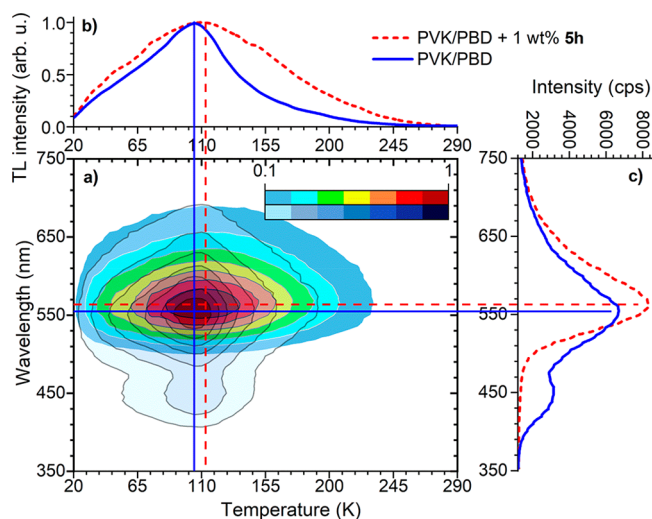


**Figure 15.** SRTL spectra for PVK/PBD layer doped with 1 wt % of emitter **5h** and for neat PVK/PBD matrix layer: (a) the TL maps; (b) normalized monochromatic TL curves recorded at  $\lambda = 565$  and  $550$  nm, respectively; (c) non-normalized isothermal spectra of emitted light recorded at 105 and 115 K, respectively. The red dashed and blue solid curves show results for the doped and neat PVK/PBD matrixes, respectively. Straight lines on the TL maps indicate selected wavelength for monochromatic TL curves (horizontal lines) and selected temperature for isothermal spectra of emitted light (vertical lines).

wavelength band; the main emission band is slightly red-shifted by 15 nm and has a smaller full width at half-maximum (FWHM). Considering the differences, it can be assumed that in doped film the emission from **5h** dominates over PVK/PBD emission. It is clear that the TL intensity of PVK/PBD with 1 wt % of **5h** is significantly higher than the TL intensity of the matrix alone (about 30%). In addition, two normalized monochromatic TL curves shown in Figure 15b differ as well. The monochromatic TL curve of the pure matrix (recorded at  $\lambda = 550$  nm) has a main maximum at 105 K. Introduction of 1 wt % of **5h** causes an increase in the relative intensity of the TL signal in the high temperature range (above 110 K), as well as TL signal broadening in comparison to that of its pure matrix analogue. In this case, high-temperature TL signal contribution was greater in comparison to the previous TL results obtained for the system doped with the iridium complex containing one fluorine atom in the *para* position of phenyl ring of the  $\beta$ -ketoiminato ligand.<sup>10</sup> This comparison points out the impact of deep traps located on the emitter molecules. The depth of the traps might be approximated to 0.5 eV for holes and 0.4 eV for electrons, on the basis of differences between HOMO and LUMO levels of the emitter (5.3 and 2.8 eV, see Table 1) and the matrix (PVK (5.8, 2.2 eV) and PBD (6.2, 2.4 eV)). However, it should be taken into account that HOMO and LUMO levels obtained from CV experiments might be slightly varied in thin films due to different environment of the molecules (THF as solvent in CV, PVK/PBD in thin films).

It can be concluded that introduction of the iridium complex molecules to PVK/PBD matrix causes formation of new, deeper trapping states that promote radiative recombination on the dopant molecules. In addition, it must be emphasized that the spectrum observed in the TL experiment for PVK/PBD doped with **5h** shown in Figure 15c is similar to the EL spectrum, as far as their shapes and location of the maximum

are concerned (cf. Figure 10b). This indicates that in both cases, after optical excitation at low temperatures (SRTL) and during the excitation induced by the current flow at room temperature (EL), the generation mechanism of triplet exciton for the emitter molecules added to PVK/PBD is similar.

## CONCLUSIONS

In summary, we reported a synthetic protocol for the obtaining of heteroleptic  $[\text{Ir}(\text{bzq})_2(\text{MeC}(\text{=NR})\text{CH}=\text{C}(-\text{O})\text{Me})]$  complexes series and studied their electrochemical, photoluminescent, and electroluminescent properties in reference to the structure of  $\beta$ -ketoiminato ligand. The spectrum of investigated R substituents included phenyl with methoxy, cyano, nitro, and 5-methyl-2-benzothiazyl groups in *para* position, as well as all possible regioisomers of naphthyl and anthracenyl moieties. In the case of nitro-substituted complexes, also *ortho* and *meta* isomers were investigated in order to explore in detail their outstanding electrochemical properties. Namely, it was found that the presence of nitro group drastically increases electron affinity. With the aid of theoretical calculations, we proved that this phenomenon was related to the reduction of nitro group and should have rather minor effect on other properties related to the bandgap between the orbitals involved in excitation and emission. Apart from the three nitro-derived complexes, the variation of ancillary ligand structure had only slight impact on the electron affinity and ionization potential.

The photoluminescence studies confirmed the results obtained from electrochemical measurements and theoretical considerations, showing that the ancillary ligand structure modification does not affect the bandgap. As a result, the complexes were found to be green emitters with emission maximum within the range of 30 nm. Surprisingly, it evidenced that the electrochemically determined bandgap for nitro-derived complexes was flawed because of the incorporation of lowest unoccupied orbital of nitro moiety. Therefore, together with theoretical calculations, it proved that HOMO localized mostly on iridium and cyclometalating ligands, and LUMOs present mostly on bzq, are predominantly involved in radiative transitions. It also correlates with the measured photoluminescence spectra, which resemble the typical broad MLCT character of the transition. Additionally, the compounds equipped with polyaromatic substituents exhibited broad and structureless emission, whereas the complexes bearing phenyl-based substituents were characterized by structured emission. The observed structure could correspond to ligand vibrations or low energy metal–ligand vibrations. Additionally, the structured emission spectra were not observed in solid state for thin film layers of PVK/PBD doped with 1 wt % of studied complexes, suggesting that mainly MLCT states were filled by exciton transfer from the host to the guest.

We found that although the structure modification of  $\beta$ -ketoiminato ligand did not allow tuning of the maximum emission wavelength, the other properties related to luminescence efficiency were strongly affected. A particular impact was observed in the photoluminescence quantum yield of PVK/PBD layers doped with 1 wt % of the studied Ir(III) phosphors, which ranged between <1 and 18%. A similar, but less spectacular change, was observed for external quantum efficiencies of the devices based on the same emissive layer, namely from 0.01 to 3.20%. Interestingly, *N,O*-donating ligands bearing unsubstituted aromatic moiety seemed to be

more promising in the application as dopants for PhOLEDs. However, this does not include the anthracenyl substituents since incorporation of these moieties resulted in instability of the complex upon photo- and electro-excitation.

From the tested devices, the best performance showed the PhOLED doped with the complex bearing 4-(1-naphthyl)-imino-2-pentanone as an ancillary ligand. The maximum measured work parameters reached 12 cd/A for current efficiency and 16000 cd/m<sup>2</sup> for luminance. It should be emphasized that these values are quite high, considering that diodes were fabricated using solution methods and taking into account the uncomplicated device structure. For reference, a very similar OLED based on [Ir(bzq)<sub>2</sub>(acac)] exhibited the maximum current efficiency of 4.2 cd/A. In all the examined devices, the electroluminescence spectra demonstrated only the dopant emission, while a significant contribution of the PVK/PBD matrix emission was observed in the photoluminescence of the same emissive layers. This indicated that the charge trapping might be the dominant mechanism of exciton generation in EL phenomenon. In fact, spectrally resolved thermoluminescence studies for the most efficient host–guest system proved that the recombination centers are created on the emitter molecules which simultaneously act as deeper trapping states, than the pure matrix. Therefore, on the basis of our results, it can be concluded that the introduction of the iridium complexes into the matrix causes efficient exciton creation on the emitter molecules in EL phenomenon, proving their applicability in PhOLED technology.

## ■ EXPERIMENTAL SECTION

**General Information.** All syntheses and manipulations were carried out under argon using standard Schlenk-line and vacuum techniques. The microwave-assisted reactions were performed with the use of a CEM Discover microwave pressure system (power max 300 W, magnetron frequency 2455 MHz, pressure max 20 bar). The chemicals were obtained from the following sources: IrCl<sub>3</sub>·3H<sub>2</sub>O from Pressure Chemicals, acetone, acetylacetone (acacH), Et<sub>2</sub>O, MeOH, CDCl<sub>3</sub>, CD<sub>2</sub>Cl<sub>2</sub>, 1,2-dichloroethane, THF, arylamines from Aldrich, benzo[*h*]quinoline (bzqH) from ABCR, THF 99.5 extra dry from Acros Organics, Bu<sub>4</sub>NBF<sub>4</sub> (purity > 98) from TCI. The complex [Ir(μ-Cl)(bzq)<sub>2</sub>]<sub>2</sub> (4)<sup>28</sup> was synthesized according to the published method. All solvents and liquid reagents were dried and distilled under argon prior to use. The NMR spectra for 4-arylimino-2-pentanones were recorded in CDCl<sub>3</sub> on 300 MHz spectrometer at 298 K, using SiMe<sub>4</sub> as internal standard for <sup>1</sup>H and <sup>13</sup>C measurements. For iridium complexes, the chemical shifts were referred to the residual protonated solvent peaks (<sup>1</sup>H δ<sub>H</sub> = 7.26 ppm for CDCl<sub>3</sub> and <sup>1</sup>H δ<sub>H</sub> = 5.32 ppm for CD<sub>2</sub>Cl<sub>2</sub>). The purity of iridium materials was determined by elemental analysis on Flash 2000 (Thermo Scientific). HRMS data were obtained on AMD 402 two-sector mass spectrometer of B/E geometry (EI-MS) and Waters/Micromass Q-tof Premier mass spectrometer equipped with an electrospray ion source (ESI-MS).

**Synthesis of Ligands and Complexes.** Detailed descriptions of the preparation of ligands and complexes, as well as spectroscopic data, can be found in the Supporting Information.

**X-ray Crystallography.** Diffraction data were collected by the ω-scan technique, for 5g and 5l at 100(1) K, for 3h and 3j at 130(1) K, for 3d and 3l at room temperature on a Rigaku Xcalibur four-circle diffractometer with an Eos CCD detector and graphite-monochromated Mo Kα radiation (λ = 0.71069 Å), and for 5j at room temperature on Rigaku SuperNova four-circle diffractometer with Atlas CCD detector and mirror-monochromated Cu Kα radiation (λ = 1.54178 Å). The data were corrected for Lorentz polarization as well as for absorption effects.<sup>29</sup> Precise unit-cell parameters were determined by the least-square fit of reflections of the highest

intensity, chosen from the whole experiment. The structures were solved with SHELXT<sup>30</sup> and refined with the full-matrix least-squares procedure on F<sup>2</sup> by SHELXL-2013.<sup>31</sup> All non-hydrogen atoms were refined anisotropically, in 3j all hydrogen atoms were found in difference Fourier maps, in 3h NH and OH hydrogen atoms, in 3d al but methyl group, and these hydrogen atoms were freely, isotropically refined. All other hydrogen atoms were placed in idealized positions and refined as “riding model” with isotropic displacement parameters set at 1.2 (1.5 for methyl groups) times U<sub>eq</sub> of appropriate carrier atoms. In the structure 3h the hydrogen atoms of methyl group C1 were found in two alternative positions with 50/50 site occupations.

The structures of two other compounds (5f and 5i) were also confirmed by X-ray diffraction, but—due to the poor quality of crystals and severe disorder—these structures are attached as Supporting Information. Table 1S lists the relevant information about the crystal and refinement data.

Crystallographic data for the structural analysis have been deposited with the Cambridge Crystallographic Data Centre, Nos. CCDC 1865881 (3d), 1892376 (3h), 1865882 (3j), 1865883 (3l), 1865883 (5f), 1865885 (5g), 1865886 (5i), 1865887 (5j) and 1865888 (5l). Copies of this information may be obtained free of charge from The Director, CCDC, 12 Union Road, Cambridge, CB2 1EZ, UK. Fax: + 44(1223)336-0333. E-mail: deposit@ccdc.cam.ac.uk. www.ccdc.cam.ac.uk.

**Thermogravimetric Analysis (TGA).** Thermogravimetric analysis (TGA) of the prepared complexes samples was carried out using a Q50-TGA thermobalance (TA Instruments, Inc.) under an N<sub>2</sub> flow of 60 mL min<sup>-1</sup>. Samples (3–5 mg) loaded on a platinum pan were heated from RT to 1000 °C at a rate of 10 °C min<sup>-1</sup>.

**Electrochemical Measurements.** Electrochemical properties were estimated from cyclic voltammetry (CV) measurement using Electrochemical Analyzer model 620 (CH Instruments). A classic three electrode setup was used with a platinum wire as a working electrode, platinum spiral as a counter electrode, and silver wire as pseudo-reference electrode. Potential was calibrated by ferrocene as an internal standard. Measurement was carried out in THF with Bu<sub>4</sub>NBF<sub>4</sub> as a supporting electrolyte. Oxidation onset potential (E<sub>ox onset</sub>) and reduction onset potential (E<sub>red onset</sub>) were estimated from the intersections of tangential lines of redox peaks and background line. Electrochemical energy gaps (E<sub>g</sub>) were estimated from equation E<sub>g</sub> = (E<sub>ox onset</sub> – E<sub>red onset</sub>)e<sup>-1</sup>. Ionization potential (IP) and electron affinity (EA) were estimated from equations IP = (5.1 + E<sub>ox onset</sub>)e<sup>-1</sup> and EA = (5.1 + E<sub>red onset</sub>)e<sup>-1</sup>.<sup>32</sup>

**Computational Methods.** The full optimizations of all Ir(III) complexes in their singlet ground state were carried out. Initially, the density functional theory (DFT)<sup>33</sup> with B3LYP—the hybrid Becke’s three parameter functional—and Lee–Young–Parr exchange–correlation potential were used.<sup>34–36</sup> For the Ir metal center the SDD basis set with Stuttgart–Dresden pseudopotentials<sup>37</sup> were used and the 6-31G(d) basis set for H, C, N, and O atoms.<sup>38</sup> After preliminary calculations more flexible basis sets including diffuse and polarization functions were used variety 6-311++G(d,p). The DFT calculations using the B3LYP,<sup>34,36,36</sup> M06,<sup>39</sup> WB97XD<sup>40</sup> functionals based on the optimized S<sub>0</sub> geometries were performed to obtain the energies of the highest occupied molecular orbital (HOMO) and the lowest unoccupied orbital (LUMO). To investigate solvent effect, the ground–state geometry optimization of iridium compounds was also performed within the SCRf (self-consistent reaction field) theory using the polarized continuum model (PCM)<sup>41–43</sup> in chlorobenzene (C<sub>6</sub>H<sub>5</sub>Cl) solution to model the interaction with the solvent. All calculations were performed using the Gaussian09 software package in PL-Grid infrastructure.<sup>44</sup>

**Spectroscopic Measurements.** Photophysical studies of new Ir complexes were performed in a solution as well as for emissive layers. All compounds were diluted (~10<sup>-5</sup> M) in chlorobenzene and the standard 1 cm path length quartz cuvette was used. Thin films (60 nm) of PVK/PBD blends (7:3 weight ratio) doped with iridium complexes were prepared on quartz substrates by means of spin-coating. Absorption spectra were detected by a Cary 5000 (Varian) spectrometer. The emission spectra were recorded on Edinburgh

Instruments FLS980 spectrofluorometer equipped with an integrating sphere used to determine the photoluminescence quantum yields.

Samples of thick layers (few  $\mu\text{m}$ ), required for SRTL experiments, were prepared by drop-casting from chlorobenzene solutions onto aluminum substrates in ambient conditions. The samples for SRTL studies were placed in the vacuum chamber on a thermostated holder and covered by a sapphire plate. After sample photoexcitation at 15 K for by pulsed nitrogen laser ( $\lambda = 337 \text{ nm}$ ) (PTI, model GL-3300T) the TL measurements were carried out in the temperature range of 20–300 K with heating rate of 7 K/min. Sample thermoluminescence was recorded by a detection system contained an optical collector, an optical-fiber, a Micro HR Imaging Spectrograph and a CCD 3500 camera (Horriba Jobin Yvon).

**Fabrication and Characterization of PhOLEDs.** The OLEDs were fabricated on glass substrates by means of the spin-coating technique followed by vacuum evaporation. First, the hole injection layer of poly(3,4-ethylenedioxythiophene) and poly(styrenesulfonate) mixture (PEDOT:PSS) was spin coated on an ITO anode in ambient conditions. Second, the emissive layer of PVK/PBD with 1 wt % Ir complex was spin-coated from a chlorobenzene solution in a glove box. The dopant concentration influence on the device parameters was checked only for **5h** in the range of 0.5–7 wt %. As the last step, the cathode materials were patterned through a shadow mask by physical vacuum deposition technique. The complete device stack can be written as ITO/PEDOT:PSS (20 nm)/PVK:PBD + emitter (60 nm)/Ca (20 nm)/Ag (100 nm). The device  $J-V-L$  characteristics were determined with use of Keithley 2400 source measurement unit connected with Minolta CS-200 camera. The EL spectra were recorded by the CCD 3500 camera (Horriba Jobin Yvon).

## ■ ASSOCIATED CONTENT

### ■ Supporting Information

The Supporting Information is available free of charge on the ACS Publications website at DOI: 10.1021/acs.inorgchem.9b02785.

Procedures for the synthesis of ligands and complexes, NMR spectra of the new compounds, X-ray analysis detailed data, thermal analysis curves, cyclic voltammograms, theoretical and experimental data correlation, frontier orbitals' energy levels and distributions, optimized geometry coordinates, and additional photo-physical data (PDF)

### ■ Accession Codes

CCDC 1865881–1865888 and 1892376 contain the supplementary crystallographic data for this paper. These data can be obtained free of charge via [www.ccdc.cam.ac.uk/data\\_request/cif](http://www.ccdc.cam.ac.uk/data_request/cif), or by emailing [data\\_request@ccdc.cam.ac.uk](mailto:data_request@ccdc.cam.ac.uk), or by contacting The Cambridge Crystallographic Data Centre, 12 Union Road, Cambridge CB2 1EZ, UK; fax: +44 1223 336033.

## ■ AUTHOR INFORMATION

### ■ Corresponding Authors

\*E-mail: [irekk@o365.amu.edu.pl](mailto:irekk@o365.amu.edu.pl).

\*E-mail: [gabriela.wiosna-salyga@p.lodz.pl](mailto:gabriela.wiosna-salyga@p.lodz.pl).

### ■ ORCID

Ireneusz Kownacki: 0000-0002-5445-760X

Maciej Kubicki: 0000-0001-7202-9169

Przemyslaw Ledwon: 0000-0001-6769-8739

### ■ Notes

The authors declare no competing financial interest.

## ■ ACKNOWLEDGMENTS

This work was supported by the National Science Centre (Poland) through grant no. UMO-2013/11/B/ST5/01334. This research was supported in part by the PL-Grid Infrastructure. E.W. acknowledges the financial support of the National Science Centre (Poland) through the grant no. UMO-2017/24/T/ST5/00017.

## ■ REFERENCES

- (1) Tang, C. W.; Vanslyke, S. A. Organic electroluminescent diodes. *Appl. Phys. Lett.* **1987**, *51*, 913–915.
- (2) Burroughes, J. H.; Bradley, D. D. C.; Brown, A. R.; Marks, R. N.; Mackay, K.; Friend, R. H.; Burns, P. I.; Holmes, A. B. Light-emitting diodes based on conjugated polymers. *Nature* **1990**, *347*, 539–541.
- (3) (a) Miyata, S.; Nalwa, H. S. *Organic Electroluminescent Materials and Devices*; CRC Press: London, 1997. (b) Li, Z. R. *Organic Light-Emitting Materials and Devices*; CRC Press: Boca Raton, 2015.
- (4) (a) Yersin, H. *Highly Efficient OLEDs with Phosphorescent Materials*; Wiley-VCH Verlag GmbH and KgaA: Weinheim, 2008. (b) Zysman-Colman, E. *Iridium(III) in optoelectronic and photonic applications*; John Wiley & Sons: Newark, 2017; pp 753.
- (5) Lamansky, S.; Djurovich, P.; Murphy, D.; Abdel-Razzaq, F.; Kwong, R.; Tsyba, I.; Bortz, M.; Mui, B.; Bau, R.; Thompson, M. E. Synthesis and characterization of phosphorescent cyclometalated iridium complexes. *Inorg. Chem.* **2001**, *40*, 1704–1711.
- (6) (a) Ko, S. H. *Organic light emitting diode—material, process and devices*; InTech: London, 2011. (b) Pereira, L. F. R. *Organic light emitting diodes: the use of rare earth and transition metals*; CRC Press, Hoboken, 2012. (c) Chi, Y.; Chang, T.-K.; Ganesan, P.; Rajakannu, P. Emissive bis-tridentate Ir(III) metal complexes: Tactics, photophysics and applications. *Coord. Chem. Rev.* **2017**, *346*, 91–100.
- (7) Perepichka, D. F.; Meng, H.; Ling, M.-M. Phosphorescent Polymer Light-Emitting Diodes. In *Organic Light-Emitting Materials and Devices*; Li, Z., Meng, H., Eds.; Taylor and Francis: Boca Raton, 2007; pp 413–449.
- (8) Xu, H.; Chen, R.; Sun, Q.; Lai, W.; Su, Q.; Huang, W.; Liu, X. Recent progress in metal-organic complexes for optoelectronic applications. *Chem. Soc. Rev.* **2014**, *43*, 3259–3302.
- (9) (a) Chen, S.; Wu, Q.; Kong, M.; Zhao, X.; Yu, Z.; Jia, P.; Huang, W. On the origin of the shift in color in white organic light-emitting diodes. *J. Mater. Chem. C* **2013**, *1*, 3508–3524. (b) Glowacki, I.; Szamel, Z.; Wiosna-Salyga, G. Spectrally resolved thermoluminescence versus electroluminescence spectra of PVK doped with 1 wt % of Ir(btpp)<sub>2</sub>(acac). *Org. Electron.* **2016**, *31*, 127–135.
- (10) Witkowska, E.; Wiosna-Salyga, G.; Glowacki, I.; Orwat, B.; Oh, M.-j.; Kownacki, I.; Kubicki, M.; Gierczyk, B.; Dutkiewicz, M.; Cieszko, P.; Luszczynska, B.; Ulanski, J.; Grzelak, I.; Hoffmann, M.; Ledwon, P.; Lapkowski, M. Effect of fluorine substitution of the  $\beta$ -ketoiminate ancillary ligand on photophysical properties and electroluminescence ability of new iridium(III) complexes. *J. Mater. Chem. C* **2018**, *6*, 8688–8708.
- (11) (a) Radwan, Y. K.; Maity, A.; Teets, T. S. Manipulating the excited states of cyclometalated iridium complexes with  $\beta$ -ketoiminate and  $\beta$ -diketiminato ligands. *Inorg. Chem.* **2015**, *54*, 7122–7131. (b) Maya, R. A.; Maity, A.; Teets, T. S. Fluorination of cyclometalated iridium  $\beta$ -ketoiminate and  $\beta$ -diketiminato complexes: extreme redox tuning and ligand-centered excited states. *Organometallics* **2016**, *35*, 2890–2899. (c) Lai, P.-N.; Brysacz, C. H.; Alam, M. K.; Ayoub, N. A.; Gray, T. G.; Bao, J.; Teets, T. S. Highly efficient red-emitting bis-cyclometalated iridium complexes. *J. Am. Chem. Soc.* **2018**, *140*, 10198–10207.
- (12) Citti, C.; Battisti, U. M.; Ciccarella, G.; Maiorano, V.; Gigli, G.; Abbate, S.; Mazzeo, G.; Castiglioni, E.; Longhi, G.; Cannazza, G. Analytical and preparative enantioseparation and main chiroptical properties of Iridium(III) bis(4,6-difluorophenylpyridinato)-picolinato. *J. Chromatogr. A* **2016**, *1467*, 335–346.
- (13) Da Silva, M. A. V. R.; Da Silva, M. D. M. C. R.; Paiva, J. P. A.; Nogueira, I. M. C. S.; Damas, A. M.; Berkley, J. V.; Harding, M. M.;

Akello, M. J.; Pilcher, G. Thermochemical and Crystallographic Studies of some p-Ketoimine Derivatives. *J. Chem. Soc., Perkin Trans. 2* **1993**, 1765–1769.

(14) (a) Gavezzotti, A. Are Crystal Structures Predictable? *Acc. Chem. Res.* **1994**, *27*, 309–314. (b) Gavezzotti, A.; Filippini, G. J. Geometry of the intermolecular X-H...Y (X, Y = N, O) hydrogen bond and the calibration of empirical hydrogen-bond potentials. *J. Phys. Chem.* **1994**, *98*, 4831–4837.

(15) Chepelin, O.; Ujma, J.; Wu, X.; Slawin, A. M. Z.; Pitak, M. B.; Coles, S. J.; Michel, J.; Jones, A. C.; Barran, P. E.; Lusby, P. J. Luminescent, Enantiopure, Phenylatopyridine Iridium-Based Coordination Capsules. *J. Am. Chem. Soc.* **2012**, *134*, 19334–19337.

(16) (a) Ràfols-Ribé, J.; Will, P.-A.; Hänisch, C.; Gonzalez-Silveira, M.; Lenk, S.; Rodríguez-Viejo, J.; Reineke, S. High-performance organic light-emitting diodes comprising ultrastable glass layers. *Sci. Adv.* **2018**, *4* (5), 1–9. (b) Kwak, K.; Cho, K.; Kim, S. Analysis of thermal degradation of organic light-emitting diodes with infrared imaging and impedance spectroscopy. *Opt. Express* **2013**, *21*, 29558–29559.

(17) Chen, Z.-Q.; Shen, X.; Xu, J.-X.; Zou, H.; Wang, X.; Xu, Y.; Zhu, D.-R. Iridium(III) complexes based on 5-nitro-2-(2',4'-difluorophenyl)pyridyl: Syntheses, structures and photoluminescence properties. *Inorg. Chem. Commun.* **2015**, *61*, 152–156.

(18) Hirva, P.; Haukka, M.; Jakonen, M.; Moreno, M. A. DFT tests for group 8 transition metal carbonyl complexes. *J. Mol. Model.* **2008**, *14*, 171–181.

(19) Skorka, L.; Filapek, M.; Zur, L.; Malecki, J. G.; Pisarski, W.; Olejnik, M.; Danikiewicz, W.; Krompiec, S. Highly Phosphorescent Cyclometalated Iridium(III) Complexes for Optoelectronic Applications: Fine Tuning of the Emission Wavelength through Ancillary Ligands. *J. Phys. Chem. C* **2016**, *120*, 7284–7294.

(20) Kodate, S.; Suzuka, I. Assignments of Lowest Triplet State in Ir Complexes by Observation of Phosphorescence Excitation Spectra at 6 K. *Jpn. J. Appl. Phys.* **2006**, *45*, 574–578.

(21) (a) Li, J.; Djurovich, P. I.; Alleyne, B. D.; Yousufuddin, M.; Ho, N. N.; Thomas, J. C.; Peters, J. C.; Bau, R.; Thompson, M. E. Synthetic Control of Excited-State Properties in Cyclometalated Ir(III) Complexes Using Ancillary Ligands. *Inorg. Chem.* **2005**, *44*, 1713–1727. (b) Yersin, H.; Rausch, A. F.; Czerwieniec, R.; Hofbeck, T.; Fischer, T. The triplet state of organo-transition metal compounds. Triplet harvesting and singlet harvesting for efficient OLEDs. *Coord. Chem. Rev.* **2011**, *255*, 2622–2652.

(22) Hsu, C.-C.; Lin, C.-C.; Chou, P.-T.; Lai, C.-H.; Hsu, C.-W.; Lin, C.-H.; Chi, Y. Harvesting Highly Electronically Excited Energy to Triplet Manifolds: State-Dependent Intersystem Crossing Rate in Os(II) and Ag(I) Complexes. *J. Am. Chem. Soc.* **2012**, *134*, 7715–7724.

(23) You, Y.; Nam, W. Photofunctional triplet excited states of cyclometalated Ir(III) complexes: beyond electroluminescence. *Chem. Soc. Rev.* **2012**, *41*, 7061–7084.

(24) Kawamura, Y.; Goushi, K.; Brooks, J.; Brown, J. J.; Sasabe, H.; Adachi, C. 100% phosphorescence quantum efficiency of Ir(III) complexes in organic semiconductor films. *Appl. Phys. Lett.* **2005**, *86*, 071104–3.

(25) Wu, L.-L.; Tsai, S.-H.; Guo, T.-F.; Yang, Ch.-H.; Sun, I.-W. Synthesis and green electrophosphorescence of a novel cyclometalated iridium complex in polymer light-emitting diodes. *J. Lumin.* **2007**, *126*, 687–694.

(26) Tang, H.; Li, Y.; Wei, C.; Chen, B.; Yang, W.; Wu, H.; Cao, Y. Novel yellow phosphorescent iridium complexes containing a carbazole–oxadiazole unit used in polymeric light-emitting diodes. *Dyes Pigm.* **2011**, *91*, 413–421.

(27) Glowacki, I.; Szamel, Z. The impact of 1 wt% of Ir(ppy)<sub>3</sub> on trapping sites and radiative recombination centres in PVK and PVK/PBD blend seen by thermoluminescence. *Org. Electron.* **2015**, *24*, 288–296.

(28) (a) Sprouse, S.; King, K. A.; Spellane, P. J.; Watts, R. J. Photophysical effects of metal-carbon  $\sigma$  bonds in ortho-metallated complexes of iridium(III) and rhodium(III). *J. Am. Chem. Soc.* **1984**,

*106*, 6647–6653. (b) Nonoyama, M. Benzo[h]quinolin-10-yl-N Iridium(III) Complexes. *Bull. Chem. Soc. Jpn.* **1974**, *47*, 767–768.

(29) CrysAlisPro (Version 1.171.38.41), Rigaku OD, 2015.

(30) Sheldrick, G. M. SHELXT – Integrated space-group and crystal-structure determination. *Acta Crystallogr., Sect. A: Found. Adv.* **2015**, *A71*, 3–8.

(31) Sheldrick, G. M. Crystal structure refinement with SHELXL. *Acta Crystallogr., Sect. C: Struct. Chem.* **2015**, *C71*, 3–8.

(32) Cardona, C. M.; Li, W.; Kaifer, A. E.; Stockdale, D.; Bazan, G. C. Electrochemical Considerations for Determining Absolute Frontier Orbital Energy Levels of Conjugated Polymers for Solar Cell Applications. *Adv. Mater.* **2011**, *23*, 2367–2371.

(33) Becke, A. D. Density-functional thermochemistry. III. The role of exact exchange. *J. Chem. Phys.* **1993**, *98*, 5648–5652.

(34) Stephens, P. J.; Devlin, F. J.; Chabalowski, C. F.; Frisch, M. J. Ab Initio Calculation of Vibrational Absorption and Circular Dichroism Spectra Using Density Functional Force Fields. *J. Phys. Chem.* **1994**, *98*, 11623–11627.

(35) Kim, K.; Jordan, K. D. Comparison of Density Functional and MP2 Calculations on the Water Monomer and Dimer. *J. Phys. Chem.* **1994**, *98*, 10089–10094.

(36) Clark, T.; Chandrasekhar, J.; Spitznagel, G. W.; Schleyer, P. V. R. Efficient diffuse function-augmented basis sets for anion calculations. III.\* The 3-21+G basis set for first-row elements, Li–F. *J. Comput. Chem.* **1983**, *4*, 294–301.

(37) Dunning, T. H.; Hay, P. J. Gaussian Basis Sets for Molecular Calculations. In *Applications of Electronic Structure Theory*; Schaefer III, H. F., Eds.; Plenum: New York, 1976; pp 1–28.

(38) Francl, M. M.; Pietro, W. J.; Hehre, W. J.; Binkley, J. S.; Gordon, M. S.; DeFrees, D. J.; Pople, J. A. Self-consistent molecular orbital methods. XXIII. A polarization-type basis set for second-row elements. *J. Chem. Phys.* **1982**, *77*, 3654–3665.

(39) Zhao, Y.; Truhlar, D. G. The M06 suite of density functionals for main group thermochemistry, thermochemical kinetics, non-covalent interactions, excited states, and transition elements: two new functionals and systematic testing of four M06-class functionals and 12 other functionals. *Theor. Chem. Acc.* **2008**, *120*, 215–241.

(40) Chai, J.-D.; Head-Gordon, M. Long-range corrected hybrid density functionals with damped atom–atom dispersion corrections. *J. Chem. Phys.* **2008**, *128*, 084106.

(41) Cancès, E.; Mennucci, B.; Tomasi, J. A new integral equation formalism for the polarizable continuum model: Theoretical background and applications to isotropic and anisotropic dielectrics. *J. Chem. Phys.* **1997**, *107*, 3032–3041.

(42) Mennucci, B.; Tomasi, J. Continuum solvation models: A new approach to the problem of solute's charge distribution and cavity boundaries. *J. Chem. Phys.* **1997**, *106*, 5151–5158.

(43) Cossi, M.; Barone, V.; Mennucci, B.; Tomasi, J. Ab initio study of ionic solutions by a polarizable continuum dielectric model. *Chem. Phys. Lett.* **1998**, *286*, 253–260.

(44) Frisch, M. J.; Trucks, G. W.; Schlegel, H. B.; Scuseria, G. E.; Robb, M. A.; Cheeseman, J. R.; Scalmani, G.; Barone, V.; Petersson, G. A.; Nakatsuji, H.; Li, X.; Caricato, M.; Marenich, A. V.; Bloino, J.; Janesko, B. G.; Gomperts, R.; Mennucci, B.; Hratchian, H. P.; Ortiz, J. V.; Izmaylov, A. F.; Sonnenberg, J. L.; Williams-Young, D.; Ding, F.; Lipparini, F.; Egidi, F.; Goings, J.; Peng, B.; Petrone, A.; Henderson, T.; Ranasinghe, D.; Zakrzewski, V. G.; Gao, J.; Rega, N.; Zheng, G.; Liang, W.; Hada, M.; Ehara, M.; Toyota, K.; Fukuda, R.; Hasegawa, J.; Ishida, M.; Nakajima, T.; Honda, Y.; Kitao, O.; Nakai, H.; Vreven, T.; Throssell, K.; Montgomery, J. A., Jr.; Peralta, J. E.; Ogliaro, F.; Bearpark, M. J.; Heyd, J. J.; Brothers, E. N.; Kudin, K. N.; Staroverov, V. N.; Keith, T. A.; Kobayashi, R.; Normand, J.; Raghavachari, K.; Rendell, A. P.; Burant, J. C.; Iyengar, S. S.; Tomasi, J.; Cossi, M.; Millam, J. M.; Klene, M.; Adamo, C.; Cammi, R.; Ochterski, J. W.; Martin, R. L.; Morokuma, K.; Farkas, O.; Foresman, J. B.; Fox, D. J. *Gaussian 16*, Revision B.01; Gaussian, Inc.: Wallingford CT, 2016.